



Published in final edited form as:

J Physiol. 2023 June ; 601(12): 2493–2511. doi:10.1113/JP284675.

Increased Pyramidal and VIP Neuronal Excitability in Rat Primary Auditory Cortex Directly Correlates with Tinnitus Behavior

Madan Ghimire¹, Rui Cai¹, Lynne Ling¹, Kevin A. Brownell¹, Troy A. Hackett², Daniel A. Llano^{3,4,5}, Donald M. Caspary^{1,*}

¹Department of Pharmacology, Southern Illinois University School of Medicine, Springfield, Illinois 62702

²Department of Hearing and Speech Sciences, Vanderbilt University Medical Center, Nashville, Tennessee 37232

³Neuroscience Program, University of Illinois at Urbana-Champaign, Urbana, Illinois, USA

⁴Department of Molecular and Integrative Physiology, University of Illinois at Urbana-Champaign, Urbana, Illinois, USA

⁵Beckman Institute, University of Illinois at Urbana-Champaign, Urbana, Illinois, USA

Abstract

Tinnitus affects roughly 15-20% of the population while severely impacting 10% of those afflicted. Tinnitus pathology is multifactorial, generally initiated by damage to the auditory periphery, resulting in a cascade of maladaptive plastic changes at multiple levels of the central auditory neuraxis as well as limbic and non-auditory cortical centers. Using a well-established condition-suppression model of tinnitus, we measured tinnitus-related changes in the microcircuits of excitatory/inhibitory neurons onto layer 5 pyramidal neurons (PNs), as well as changes in the excitability of vasoactive intestinal peptide (VIP) neurons in primary auditory cortex (A1). Patch-clamp recordings from PNs in A1 slices showed tinnitus-related increases in spontaneous excitatory postsynaptic currents (sEPSCs) and decreases in spontaneous inhibitory postsynaptic currents (sIPSCs). Both measures could be correlated to the rat's behavioral evidence of tinnitus. Tinnitus-related changes in PN excitability were independent of changes in A1 excitatory or inhibitory cell numbers. VIP neurons, part of an A1 local circuit that can control the excitation of layer 5 PNs via disinhibitory mechanisms, showed significant tinnitus-related increases in

*Corresponding author: Donald M. Caspary, Department of Pharmacology, Southern Illinois University School of Medicine, PO Box 19629, Springfield, IL 62794-9629, dcaspary@siumed.edu.

Author Contributions

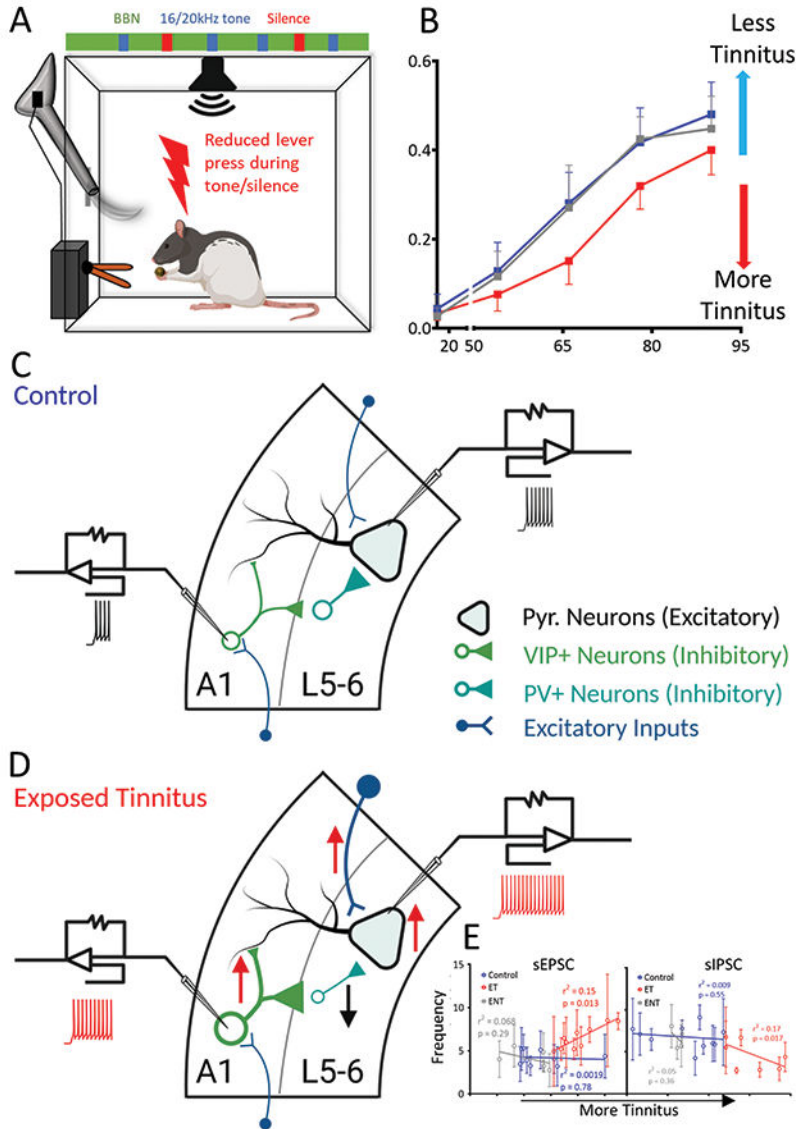
Electrophysiology and associated imaging studies carried out in DMC Neurobiology laboratories at SIU-SM. FISH studies by TAH at Vanderbilt University; MG: study design, data acquisition, data analysis, data interpretation, manuscript drafting and editing; RC: data analysis, interpretation manuscript editing; LL: Receptor binding, IHC, data collection and interpretation, manuscript editing; KB: Operant behavior, generation, training and testing tinnitus subjects; TAH: generation, interpretation analysis of FISH data, manuscript editing; DAL: study design, data interpretation, manuscript editing; DMC: study design, data analysis, data interpretation, manuscript editing. All authors have approved final version of the manuscript. DMC agrees to be accountable for all aspects of the work and will ensure that questions related to the accuracy or integrity of any part of the work are appropriately investigated and resolved.

Conflict of Interest

The authors declare no conflict of interest.

excitability that directly correlated with the rat’s behavioral tinnitus score. That PN and VIP changes directly correlated to tinnitus behavior, suggests an important role in A1 tinnitus pathology. Tinnitus-related A1 changes were similar to findings in studies of neuropathic pain in somatosensory cortex suggesting a common pathology of these troublesome perceptual impairments. Improved understanding between excitatory, inhibitory and disinhibitory sensory cortical circuits can serve as a model for testing therapeutic approaches to the treatment of tinnitus and chronic pain.

Graphical Abstract



A, B. Noise-exposed animals with behavioral evidence of tinnitus show poor ability to distinguish tone from silence. C. Whole cell patch-clamp recordings from layer 5 pyramidal neurons and (D) VIP+ GABAergic neurons showed significant tinnitus-related increases in excitatory

responses. Pyramidal neurons also showed a significant loss of inhibitory input (disinhibition). E. Collectively, tinnitus-related changes were directly correlated to the animal's tinnitus score.

Keywords

Tinnitus-related plasticity; auditory cortex; excitatory and inhibitory neurotransmission; pyramidal and VIP neurons

Introduction

Tinnitus, commonly referred to as ringing in the ears, is believed, in part, to reflect maladaptive plastic changes at various levels of the central auditory pathway as well as in non-auditory cortical areas, limbic and attentional structures. Partial deafferentation due to peripheral damage results in sensory deprivation to central auditory structures (Kujawa & Liberman, 2009; Shore & Wu, 2019; McGill et al., 2022). Canonical physiologic signs of decreased auditory input, described for tinnitus models, include increased spontaneous activity, increased neural synchrony and increased bursting at multiple levels of the central auditory pathway (Brozoski et al., 2002; Kaltenbach et al., 2004; Brozoski & Bauer, 2005; Kaltenbach et al., 2005; Ma et al., 2006; Schaette & Kempster, 2006; Bauer et al., 2008; Roberts et al., 2010; Noreña, 2011; Auerbach et al., 2014; Geven et al., 2014; Kalappa et al., 2014; Ropp et al., 2014). Markers for tinnitus-related maladaptive changes in neurotransmission are generally associated with disrupted excitatory glutamatergic and inhibitory GABA-/glycinergic signaling (Wang et al., 2009; Roberts et al., 2010; Kaltenbach, 2011; Richardson et al., 2012; Eggermont, 2013; Zhang, 2013; Sametsky et al., 2015; Caspary & Llano, 2017). The present study posited that primary auditory cortex (A1) layer (L) 5 pyramidal neurons (PNs) and vasoactive intestinal peptide (VIP) inhibitory neurons would show selective tinnitus-related changes in glutamatergic and GABAergic signaling.

Similar to somatosensory and visual cortices, the primary auditory cortex (A1) houses a complex local-circuitry of excitatory and inhibitory neurons, responsible for integration and higher order processing of sensory information (Winer & Lee, 2007; Gonchar et al., 2008; Letzkus et al., 2011; Schneider et al., 2014; Mesik et al., 2015). Deeper A1 layers are engaged in top-down modulation of ascending auditory information and integration of cortico-cortical information (Nelson et al., 2013; Williamson & Polley, 2019; Blackwell et al., 2020). In layer 5 of A1, excitatory pyramidal neurons (PNs) are found to interact in local circuits with at least 3 distinct types of inhibitory interneurons, parvalbumin (PV), somatostatin (SOM), and vasoactive intestinal peptide (VIP) neurons, located across layers (Blackwell & Geffen, 2017; Askew et al., 2019). Apical dendrites of layer 5 PNs receive mono- and polysynaptic glutamatergic excitatory ascending signals from MGB and modulating inhibitory inputs from surrounding GABAergic interneurons (Letzkus et al., 2011; Schneider et al., 2014; Mesik et al., 2015; Blackwell & Geffen, 2017; Phillips et al., 2017; Askew et al., 2019; Blackwell et al., 2020). Within A1, excitatory inputs originate from the columnar principal neurons (Barbour & Callaway, 2008), and VIP neurons regulate the excitability of layer 5 PNs through disinhibition (Pfeffer et al., 2013; Pi et al., 2013).

Activation of GABAergic PV and SOM interneurons provides direct inhibition onto PNs, while VIP interneurons, when activated inhibit PV and SOM interneurons, favoring the excitation of PNs via disinhibitory mechanisms (Letzkus et al., 2011; Pfeffer et al., 2013; Pi et al., 2013; Askew et al., 2019). Layer 5 PNs project excitatory glutamatergic information to subcortical nuclei, primarily inferior colliculus (IC), extra-lemniscal medial geniculate body (MGB) as well as to secondary auditory and non-auditory structures (Barbour & Callaway, 2008; Stebbings et al., 2014; Sottile et al., 2017; Williamson & Polley, 2019). The present studies chose to examine Layer 5 PNs and associated inhibitory micro circuitry based in part, on studies by Cichon et al. (2017) who successfully alleviated neuropathic pain by manipulating Layer 5 microcircuits in somatosensory cortex. Here we examine the impact of tinnitus on layer 5 PNs and VIP neurons. We used an established operant rat model of tinnitus in a series of whole-cell patch-clamp studies to investigate tinnitus-related synaptic changes in A1 layer 5 PNs and VIP neurons.

Methods:

Ethical Approval:

Animals were handled according to SIU-School of Medicine LAB Animal Care and Use Committee (LACUC) approved protocols SIU-SM, Protocol number 41-21-007.

Animals:

51 wild-type (WT, Envigo, Indianapolis, IN), 14 ChAT-Cre (Rat Resource & Research Center, Columbia, MO) and 19 *VIP^{Cre}:Rosa26^{tdTomato}* (Envigo, Indianapolis, IN) adult Long-Evans (LE) rats were entered into the studies at 3-4 months and used in a series of experiments at 8-10 months. Experimental details of animal usages are shown in table 1. All animals were single housed, with a restricted diet schedule starting at the time of noise-exposure until the assessment of tinnitus. A reverse light/dark cycle was maintained in order to conduct behavioral studies during active periods of the animals.

Tinnitus Induction:

To assure that all animals used in the present study had normal hearing thresholds, 3-4 months old WT, ChAT-Cre or *VIP^{Cre}:Rosa26^{tdTomato}* LE rats animals were anaesthetized using a cocktail of ketamine (90 mg/kg)/xylazine (7 mg/kg) and auditory brainstem response (ABR) thresholds were obtained before and after the exposure for pure tones at 8, 10, 12, 16, 20, 24, and 32 kHz, presented in 10 dB increments between 10 and 80 dB (SPL re 20 μ Pa). One week following ABR testing, at 3 months of age, rats were anesthetized with a 1.7% isoflurane/O₂ mixture and placed in a head holder for noise-exposure of the right ear. Rats were unilaterally exposed to narrow-band (16 kHz centered) noise for 1 hour, with a peak level of 116 dB (SPL), falling to ambient levels at 8 kHz and 24 kHz, with the contralateral canal blocked (Bauer & Brozoski, 2001). **Calibration:** Prior to each set of noise-exposures/ABRs, subsets of *in vivo* and behavioral experiments, sound levels were calibrated using a Brüel and Kjaer Pulse sound measurement system (13.1 software; 4138 microphone) (see Kalappa et al., 2014).

Tinnitus Assessment:

One week following noise-exposure, diet restricted animals were placed in an operant chamber (Lafayette Neuroscience) with attached horn tweeter (KSN 1025A Wide Dispersion Horn Tweeter, Piezosource Inc. CA) playing constant 60 dB broadband (BBN) noise and that contained a computer-controlled lever (ABET II software). Animals were trained to obtain food via lever press for 60 minutes (30 two minutes bins) operating sessions. Additional food was supplemented if the body weight dropped below 80% of *ad libitum* weight. After animals met the criteria for stable lever pressing throughout the training session, a variable interval reinforcement schedule was introduced. The variable inter-lever-press interval of 6 – 30 seconds was pseudo randomly generated by the ABET II software (Lafayette Neuroscience) for operant control, and food delivery. Each series of lever presses would deliver food pellets, if animals maintained pressing during the inter-press interval. If not, the interval would reset to the last interval without food delivery. Animals were trained on this schedule for a minimum of 2 months prior to being tested for their ability to identify silence during the testing period. Animals thought to have tinnitus were found to show behavioral defects in silence identification. The test period consisted of a total 30 two-minute sessions, composed of 4 pure tone (16/20 kHz) and 2 silent periods randomly inserted between 24 BBN periods. Rats were allowed to obtain food throughout this time, however if they pressed the lever during the silent period, a single 0.5 mA foot shock was provided at the conclusion of silence period. Foot shock provided a negative reinforcement to the animals, and they quickly modified their behavior. Animals that could identify silence suppressed lever pressing during silence period. Animals unable to identify silence from tone periods suppressed lever pressing during both silence and certain tone periods. Based on a rat lever pressing, a suppression ratio was calculated according to the formula: $R = A/(A+B)$ where R = Suppression ratio; A = lever press during 16/20 kHz tone period, and B = lever press following (two min bin) tone period. Exposed animals with mean suppression ratios smaller than 0.26 were considered exposed tinnitus. Three criteria had to be met for individual-subject data to be included for further analysis: 1) There had to be a minimum of 200 lever presses per session; 2) mean R for background noise periods (i.e., baseline performance) had to be >0.4 , with 3) a SD of <0.2 . Data from a minimum of five test sessions, for each stimulus, were averaged to derive individual and group discrimination functions for each stimulus: BBN, 16, and 20 kHz tones. Once the psychological tests were concluded, exit ABRs were collected under anesthesia (mixture of ketamine (90 mg/kg) and xylazine (7 mg/kg)).

Micro-injection surgery:

Tinnitus tested wild-type and *VIP^{Cre}:Rosa26^{tdTomato}* LE rats (8-9 months) were anaesthetized with a cocktail of ketamine (90 mg/kg)/xylazine (7 mg/kg) (induction anesthesia) followed by 0.5-1% isoflurane (maintenance). Animals were head fixed in a stereotaxic apparatus with viral vectors injected intracranially using a Neurostar stereotaxic drill and injection system (stereodrive 015.838, injectomate IM28350, stereodrill DR352; Neurostar, Germany). A midline incision was made to expose the skull. In wild-type rats, a craniotomy of 1.5 mm was drilled at AP –5.7 mm and ML –3.5 mm, corresponding to MGB injection site. A 2 μ l Hamilton micro-syringe was used to inject approximately 250-300 nl (1×10^{13} vg/ml titer concentration) of AAV5-CaMKIIa-hChR2(H134R)-EYFP (UNC Vector

Core, UNC, Chapel Hill, NC) 6mm ventral to bregma. In *VIP^{Cre}:Rosa26^{tdTomato}* rats, a craniotomy of 1.5 mm was drilled at AP -5.7 mm and ML -4.9 mm respective to bregma corresponding to A1 injection site. A 2 μ l Hamilton micro-syringe containing AAV-EF1a-DIO-hChR2(H134R)-EYFP (UNC Vector Core, UNC, Chapel Hill, NC) was fixed at -22 -degree angle in a sagittal plane. The syringe was advanced 5 mm from the surface of the brain to reach A1, and approximately 150-200 nl (1×10^{13} vg/ml titer concentration) of the virus was injected. Ibuprofen (10-15 mg/kg/24 h) was placed in drinking water one day prior and up to 4 days post-surgery. Following surgery animals were observed until fully ambulatory. Animals were allowed to recover and express the virus for a minimum of 3 weeks before being used in *in vitro* optogenetic studies.

Cortical slice electrophysiology:

LE rats (8-9 months) were anesthetized with 4% isoflurane and cardiac perfusion was performed using ice-cold sucrose aCSF (in mM as follows: 2.5 KCl, 5 MgCl₂, 1.23 NaH₂PO₄, 0.5 CaCl₂, 250 sucrose, 26 NaHCO₃, and 10 glucose, pH 7.4) saturated with carbogen (95% O₂/5% CO₂) before decapitation. After perfusion and decapitation, brains were rapidly isolated and submerged in ice-cold (1°C – 2°C) sucrose aCSF, pH \sim 7.4, and oxygen saturation was maintained by bubbling with carbogen. aCSF composition was as follows (in mM): 125 NaCl, 3 KCl, 1 MgCl₂, 1.23 NaH₂PO₄, 2 CaCl₂, 26 NaHCO₃, and 10 glucose. 5-6 coronal slices of 250–300 μ m through A1 were sectioned using a vibratome (Pelco), following previously described protocols (Richardson et al., 2013; Ghimire et al., 2020), and incubated for 15 min at 31°C. Slices were allowed to equilibrate at room temperature (20°C – 22°C) for 60 min in carbogen-bubbled aCSF before recordings. Slices were transferred to an immersion recording chamber (2 ml), perfused at 2–3 ml/min with aCSF bubbled with carbogen, and all the recordings were performed at room temperature. Layer 5 PNs were identified morphologically using QImaging Rolera bolted on a differential interference contrast microscope (BX50WI, Olympus Optical) under a 40 \times water-immersion objective. Likewise, tdTomato labeled VIP neurons were identified using fluorescence system (lambda 421, Sutter Instruments) with excitation 560 nm/emission 581 nm, attached to the DIC microscope.

In vitro patch-clamp recordings:

Once cells were identified, whole-cell patch-clamp recordings were performed using 3-6 M Ω fire-polished microfilament micropipettes, pulled from borosilicate glass (0.86 mm ID, 1.5 mm OD; Sutter Instruments). Two different compositions of the internal solution were used 1) (in mM): 140 potassium gluconate, 1 NaCl, 2 MgCl₂, 5 KCl, 10 HEPES, 2 Mg-ATP, 0.3 Na-GTP, 6.88 KOH, Osm: \sim 300 mOsm, pH 7.3 (adjusted with Tris-Base) with calculated chloride reversal potential near -65 mV and 2) (in mM) 140 CsCl, 2 MgCl₂, 4 Mg-ATP, 0.3 Na-GTP, 10 Na-HEPES, 5 QX 314 and 0.1 EGTA, with a pH of 7.25 adjusted with HCl (osmolarity, \sim 290 mOsm), resulting in a Cl⁻ equilibrium potential (E_{Cl⁻}) value near 0 mV. Pipettes were attached to Multi-clamp 700B Amplifier (Molecular Devices), and cells recorded in current-clamp mode at $I = 0$ or voltage-clamp mode at -65 mV at 10 kHz sampling rate. In all recordings using potassium gluconate based internal solution, a liquid junction potential of 15 mV was corrected, and series resistance was compensated 85-90% for voltage clamp recordings. An automatically calculated bridge balance was applied in

current clamp recordings. The patch pipette was attached to layer 5 PN or layer 2/3 VIP neurons with Giga-ohm ($> 4 \text{ G}\Omega$) seal and the membrane was ruptured with a brief sharp suction. Whole-cell recordings were collected with access resistances ranging from 10-25 $\text{M}\Omega$. Whole-cell capacitance, input resistance, and access resistance were determined by injection of a 5-mV square pulse, at 20 Hz. Exclusion criteria included the following: 1) a resting membrane potential more depolarized than -55 mV , 2) access resistance $> 25 \text{ M}\Omega$, 3) a resting input resistance $< 100 \text{ M}\Omega$ (for PNs only). TTL pulses, voltage commands, acquisition, and display of the recorded signals were achieved with Axon Digidata 1440A (Molecular Devices) using the Clampex 10.7 program without application of any filters.

Optogenetic studies: Optogenetic studies used adult (8-10 months) wild-type and *VIP^{Cre}:Rosa26^{tdTomato}* rats that underwent viral injection at MGB or A1. 50 ms pulses of blue light (470 nm) were used to activate ChR2 with a ThorLabs fiber coupled LED (M470F4) with an attached 400 μm diameter fiber tip. The power of the illumination was determined to be 1.42 mW/mm^2 at the tip of the fiber. The tip of the fiber was positioned approximately 1-2 mm above the brain slice with illumination directed at the area of interest.

Saturation Binding:

Binding protocols were identical to those used previously (Richardson et al., 2011; Ling & Caspary, 2013). Five control and five noise-exposed LE rats (8-10 months) were decapitated, and the brains were rapidly isolated, rinsed in ice-cold phosphate buffer at 4°C , pH 7.4, frozen in powdered dry ice, and stored at -80°C . Serial transverse sections were cut at $16 \mu\text{m}$ using a Leica CM1850 cryostat at -24°C . Selected sections were thaw-mounted onto Superfrost/Plus slides and stored at -20°C . Anatomical locations of the A1 were verified to match neural structures with those described previously (Paxinos & Watson, 1998).

[^3H]gaboxadol (GBX) (a gift from Merck, Inc.) was used with modified protocols from Dr. Bjarke Ebert (H. Lundbeck A/S, Copenhagen, DK; personal communication) as described in Richardson et al. (2011). After fixed in 4% PFA for 10 minutes at room temperature, tissue sections were subjected to prewash twice for 5 min in buffer, followed by incubation with [^3H] gaboxadol: 10–400 nM for 1 hour at 4°C and post-wash with buffer for four quick dips. The buffer solution used was 50 mM Tris-citrate, pH 7.1. Nonspecific binding was determined in adjacent sections by the addition of cold excessive GABA to the ligand buffer and was subtracted from total binding.

Dried slides were opposed to [^3H]-hypersensitive phosphor screens for 2 d at room temperature. The phosphor screens were scanned using a Cyclone Storage Phosphor System (PerkinElmer). Layers 2-6 of A1 were outlined and analyzed using OptiQuant Image Analysis software (Canberra Packard), which provided tools for grayscale quantification in digital light units. Digital light units were then converted to nanocuries per milligram protein using a standard curve generated from co-exposed [^3H]-embedded plastic standards (American Radiolabeled Chemicals). GraphPad Prism software was used for data analysis and generating graphs.

Cellular phenotyping and quantification: Multiplexed fluorescence in situ hybridization (FISH) was used to identify neuronal cell types in fresh frozen tissue sections

(14 μm) across AI layers. Cells were identified by detection of cell-type-specific markers for excitatory neurons (VGluT1, Slc17a7), and inhibitory neurons (VGAT, *Slc32a1*) with their subtypes (parvalbumin, *Pvalb*; vasoactive intestinal peptide, *Vip*; somatostatin, *Som*) in the same tissue sections, counterstained with DAPI. Assays were conducted in sections collected from primary auditory cortex (A1) of 5 animals in each experimental group using custom RNAscope riboprobes and detection kits manufactured by Advanced Cell Diagnostics (Newark, CA), as in prior studies from our lab (Ghimire et al., 2020). Sections were imaged at 20x using a Nikon 90i epifluorescence microscope, permitting selective detection of transcripts for each cell marker by color channel. Images were imported in HALO pathology software (Indica labs, Albuquerque, NM) for analysis. Cells expressing the transcripts of each cell marker were separately tallied in each layer of A1 (Table 2).

Statistical and data analysis

Signals obtained from electrophysiological recordings were filtered post hoc at 5 kHz lowpass Gaussian filter and sEPSCs and sIPSCs were isolated via template fit using Clampfit 10.7 (Molecular Devices). Correlation across control and ET animals in different groups (entering studies at different times) was established using z-score as a function of tinnitus score. z-scores ($z\text{-score} = (\text{observed value} - \text{mean}) / \text{standard deviation}$) were calculated when tinnitus scores from tested animals in different entering groups were combined. Statistical analysis was performed using GraphPad Prism 9, with corresponding statistical tests matched to the data noted in the figure legends. All graphs represent mean \pm SD. Student's *t*-tests were used for individual sample comparison and a one-way/two-way ANOVA with a Bonferroni *post hoc* correction was used for multiple comparisons. Data were tested for the homogeneity of variance, and *p* values corrected based on statistical significance. All comparisons with *p* value < 0.05 were considered significant.

Results:

Subjects in the present study were tested for changes in their acoustic threshold using the auditory brainstem-evoked response (ABR). ABR threshold changes in unexposed/control rats were compared with right ear/unilaterally noise-exposed Long Evans (LE) rats, which showed modest threshold shifts at frequencies adjacent to the 16 kHz exposure frequency at the end of the tinnitus test paradigm (3-4 months after exposure) (Fig. 1A). As detailed in the Methods, noise-exposed animals were parsed into two groups (exposed tinnitus (ET), exposed non-tinnitus (ENT)) based on their behavioral suppression ratios indicative of psychophysical evidence of tinnitus (Fig. 1B, C). Tinnitus suppression scores were converted to z-scores to normalize suppression ratios across different sets/groups of rats studied over the course of the 3 years. Tinnitus testing occurred 3-4 months following noise-exposure (6-7 months. of age) with 50-60% of noise-exposed rats showing behavioral evidence of tinnitus. Approximately 90% of control/unexposed animals showed near-base-level suppression ratios/non-tinnitus behavior (Fig. 1B, C). The third group of noise-exposed rats showed control-like behavior suggesting little evidence of tinnitus and were classified as exposed non-tinnitus (ENT) (Fig. 1B, C). *In vitro* recordings were obtained from whole-cell patch-clamped neurons (200 PNs and 50 VIP interneurons) in A1 slices from 30 ET, 11 ENT

and 26 unexposed-Ctrl rats (Table 1). A1 cell counts were obtained using fluorescence *in situ* hybridization from 5 control and 5 ET animals.

A1 layer 5 PN showed tinnitus-related increases in activity of glutamatergic input neurons.

Whole-cell patch-clamp electrophysiology from 9 control, 11 ET, and 4 ENT rats was used to examine tinnitus-related changes in the physiology of A1 layer 5 PNs (Fig. 2A). The chloride reversal potential was -65 mV, and voltage clamp recordings were collected at -65 mV with current clamp recordings collected at $I = 0$. Once whole-cell configuration was achieved, intrinsic properties including resting membrane potentials (RMP) and rheobase current (RC) were measured after the cell stabilized, typically after 2-3 minutes. Resting membrane potential of layer 5 PNs was found to be significantly depolarized in ET animals, while no measurable difference was observed in ENT animals compared to control PNs (Fig. 2B). There were no tinnitus-related changes in rheobase current (RC, current required to evoke an action potential) between groups (Mean \pm SD pA, Control, 74.33 ± 26.48 , $n = 30$; ET, 73.26 ± 29.98 , $n = 43$; ENT, 87.14 ± 47.51 , $n = 23$, $F(2, 77) = 0.63$, $p = 0.53$, graph not shown). To assess the activity of excitatory input neurons, we collected continuous voltage-clamp recordings of the frequency and amplitude of depolarizing sEPSCs from layer 5 PNs (Fig. 2C). Layer 5 PNs from ET rats showed significant tinnitus-related increases in sEPSC frequency, with no significant sEPSC frequency changes observed in ENT rats (Fig. 2D). ET animals showed a linear relationship between the sEPSC frequency and normalized tinnitus score (z-score). This relationship was not significant for Ctrl and ENT animals (Fig. 2E). No significant changes in sEPSC peak amplitude were observed from the PNs of control, ET and ENT animals (Fig. 2F, G).

A1 layer 5 PN show tinnitus-related increases in thalamocortical excitability.

Layer 5 PNs receive glutamatergic inputs from thalamocortical neurons and indirect excitatory connections from within and outside A1 (Huang & Winer, 2000; Banks & Smith, 2011). MGB is the primary source of ascending excitatory auditory input to A1 terminating throughout A1 layers with largest projections to layers 1 and layer 4 (Huang & Winer, 2000; Banks & Smith, 2011; Takesian et al., 2018). Apical dendrites emerge from layer 5 PNs and ascend throughout granular and supragranular layers of A1 while receiving mono and polysynaptic thalamocortical endings (Slater et al., 2019). Tinnitus-related changes in the ascending MGB inputs onto layer 5 PNs were examined using optical stimulation of thalamocortical terminals in A1 (Fig. 3A). We injected AAV-ChR2 in the MGB and allowed the virus to express for 3-4 weeks. Acute slices of (~ 250 - 300 μm) were prepared and whole-cell patch-clamp recordings were performed. The expression of virus in the MGB neurons was confirmed by imaging the slices containing MGB and A1 for the presence of fluorophore EYFP (Fig. 3B). Thalamocortical endings appeared most prominent in layers 1 and 4 of A1 (Fig. 3B). Optical stimulation of thalamocortical terminals evoked significantly larger depolarizing currents (EPSCs) from PNs in ET animals with behavioral evidence of tinnitus than from PNs from control animals (Fig. 3C, D). Optical stimulation of thalamocortical terminals evoked multiple EPSC peaks, in layer 5 PNs from both control and tinnitus animals suggesting the potential polysynaptic nature of the excitation. We measured the peak-two latency from the evoked EPSCs. Peak-two latency was consistent

with a polysynaptic latency, as thalamocortical response latencies are typically shorter than 5 milliseconds (Gil & Amitai, 1996). We also observed a significant tinnitus related decrease in peak-two latency, likely reflecting increased glutamatergic release (Boudkkazi et al., 2007). Observation of tinnitus-related increases in thalamocortical excitability is suggestive of tinnitus-related plastic changes in both local A1 excitatory neurons and the thalamocortical projection.

A1 layer 5 PNs show tinnitus-related decreases in GABAergic inhibitory input.

Whole-cell patch-clamp electrophysiology from 10 control, 10 ET, and 5 ENT rats was used to examine tinnitus-related changes in the physiology of A1 layer 5 PNs. Increased A1 excitability may, in part, reflect direct and/or indirect loss of synaptic inhibition within A1. SOM, PV and VIP interneurons represent the primary sources of GABAergic inhibition in A1 microcircuitry (Gonchar et al., 2008; Blackwell & Geffen, 2017). Spontaneous GABAergic inhibitory currents (sIPSCs) were collected from layer 5 PNs in continuous whole-cell recordings from controls and animals with behavioral evidence of tinnitus (Fig. 4A). Recordings were collected in the presence of bath DNQX and AP5 to block the influence of AMPA and NMDA receptors, respectively. There was a significant tinnitus-related decrease in sIPSCs frequency from layer 5 PNs in ET animals, while layer 5 PNs from ENT animals showed no decrease in sIPSC frequency when compared to control animals (Fig. 4A, B). ET animals showed a linear relationship between the decrease in sIPSC frequency and normalized tinnitus score (z-score), which was not seen for control and ENT animals (Fig. 4C). In addition, layer 5 PNs in ET animals showed a significant decrease in sIPSCs amplitude, while no significant difference in sIPSC amplitude was observed in recordings from layer 5 PNs from ENT animals. (Fig. 4D, E). We measured tinnitus-related changes in intrinsic/ambient GABA inhibition in layer 5 PNs by blocking GABA_AR responses with gabazine. Bath application of gabazine induced a rapid tonic change in holding current in recordings from PNs from control and ENT animals (Fig. 4F, G). This was interpreted as reflecting intrinsic GABAergic tonic inhibitory current mediated via extrasynaptic GABA_ARs. PNs from ET animals showed a significant tinnitus-related loss of tonic inhibition revealed by gabazine (Fig. 4F, G). This significant tinnitus-related loss of intrinsic GABA_A mediated tonic inhibition at layer 5 PNs likely reflects decreased availability of ambient GABA or loss of extrasynaptic receptors. Miyakawa et al., found a significant tinnitus-related loss of the GABA synthetic enzyme GAD₆₅, suggesting a possible decrease in the availability of ambient GABA in animals with evidence of tinnitus (Miyakawa et al., 2019). We used fluorescence *in situ* hybridization to identify specific populations of excitatory and inhibitory neurons in A1 from tinnitus and control rats. There were no significant tinnitus-related changes in the density of PV, SOM and VIP neurons or in excitatory (VGLUT1 positive) neurons across A1 layers (Table 2). When layer-specific changes were examined, only layer 4 PV cells from rats with behavioral evidence of tinnitus showed significant tinnitus-related decreases in cell density. Prior findings examining the impact of noise-exposure on PV cell numbers have been inconsistent, with some studies showing no change in PV cell density while other studies showed decreased or increased PV cell density (Nguyen et al., 2017; Liu et al., 2018; Miyakawa et al., 2019; Deng et al., 2020).

Tinnitus-related loss of GABA_AR function.

Tinnitus-related decreases in sIPSC amplitude may reflect changes in postsynaptic GABA_AR composition and/or function. GABAergic currents were examined in recordings from layer 5 PNs in response to puffed GABA (50 μM, 20 ms puff) 30 μm from the PN being studied (Fig. 5A, B). PNs recorded from animals with behavioral evidence of tinnitus showed significantly smaller GABA evoked current when compared to PNs recorded from control and ENT animals (Fig. 5C).

These findings from layer 5 PNs, suggest tinnitus-related changes in the number and/or subunit composition postsynaptic GABA_AR. Closer examination of GABA evoked postsynaptic currents showed significantly longer/slower rise-times (10-90% rise, Fig. 5D) in PNs from ET animals compared to control and ENT rats. Likewise, changes in GABA evoked decay/fall-times (90-10% fall, Fig. 5E) times were significantly different between ET animals compared to control and ENT animals. Altered rise-fall characteristics of evoked currents have previously been shown to reflect synaptic GABA_AR subunit changes (Schofield & Huguenard, 2007).

Extrasynaptic GABA_AR function remains relatively intact in tinnitus

animals: As described above and in Figure 4F, G, extrasynaptic GABA_ARs (α₄δ) enable neurons to sense ambient extrasynaptic GABA concentrations reflected by generation of a tonic inhibitory current (Belelli et al., 2009). Recordings from A1 layer 5 PNs showed tinnitus-related reductions in the endogenous GABA_AR inhibitory current mediated by extra-synaptic GABA_AR blockade (Fig. 6A). We asked if this tinnitus-related change in tonic GABA_AR current was due to loss of extrasynaptic GABA_ARs or a loss of ambient GABA. Bath application of the selective α₄δ GABA_AR agonist gaboxadol (GBX, 5 μM, 5 min) was used to evoke tonic GABA_AR mediated currents that plateaued after few seconds (Fig. 6A). Figure 6B shows nonsignificant tinnitus-related changes in GBX evoked GABA_AR tonic inhibitory current which suggested that tinnitus-related changes in the numbers of extrasynaptic GABA_ARs was unlikely. These results were further supported in a saturation [³H]GBX binding study comparing control and noise-exposed animals using the same noise-exposure paradigm as in the present study (Fig. 6C). Consistent with the physiology, binding in A1 contralateral to the exposed ear showed only non-significant changes in the number of [³H]GBX binding sites (B_{max}) and in the dissociation constant (K_d) (Fig. 6D, E). Together, these findings suggest the observed loss of tonic/intrinsic GABA_AR inhibition in layer 5 PNs from tinnitus rats was likely due to lowered availability of ambient GABA in A1 as suggested by previous human and animal studies (Llano et al., 2012; Sedley et al., 2015; Deng et al., 2020).

A1 VIP neurons show tinnitus-related increased excitability: Cortical VIP neurons play a key role in regulating the activity of PNs. The canonical inhibitory microcircuitry of A1 describes inhibitory VIP neurons as projecting onto inhibitory PV and SOM neurons, which in turn provide for disinhibitory regulation of layer 5 PNs (Mesik et al., 2015; Askew et al., 2019). We posited that tinnitus-related increases in VIP neuronal activity would inhibit PV and SOM neurons resulting in disinhibition of layer 5 PNs. To test this hypothesis, VIP-Cre LE rats were bred with a tdTomato reporter line of LE rats to obtain offspring

expressing tdTomato in VIP-positive neurons (Fig. 7A). Expression of tdTomato VIP neurons was immunohistochemically confirmed using an anti-VIP antibody (Fig. 7B, C). VIP x tdTomato rats were inserted into the previously described, noise-exposure/training/tinnitus testing protocol and classified as non-exposed controls or animals with behavioral evidence of tinnitus (ET). VIP neurons were identified in A1 slices using fluorescence microscopy and studied using whole-cell patch-clamp recordings as above. The intrinsic properties and excitability profile of VIP neurons from control animals were compared with neurons from ET rats. VIP neurons from ET animals were significantly depolarized compared to controls (Fig. 7D). VIP neurons from ET animals were highly excitable at significantly lower injected currents/RC (current required to generate action potential) when compared to VIP neurons from control animals (Fig. 7E, F). Injection of twice the threshold current (2XRC) evoked significantly greater numbers of action potentials (APs) from VIP neurons in ET animals (Fig. 7G).

Discussion:

The present studies found significant tinnitus-related maladaptive plastic changes in A1 layer 5 PNs and VIP inhibitory neurons in an established behavioral rat model of tinnitus. 1) Layer 5 PNs from ET animals were significantly depolarized at rest, reflecting a disrupted excitatory-inhibitory balance. 2) Layer 5 PNs displayed increased frequency of sEPSCs and decreased frequency of inhibitory currents (sIPSCs) with these tinnitus-related changes directly correlated to the severity of the rat's tinnitus behavioral score. 3) Postsynaptic GABA_ARs showed tinnitus-related reductions in their responses to GABA, suggestive of decreases in GABA_AR expression or altered subunit make-up of GABA_ARs (Wafford et al., 1993). 4) Layer 5 PNs showed enhanced thalamocortically evoked polysynaptic EPSCs in ET animals. Previous studies describe tinnitus-related changes suggestive of increases in the number of active ascending MGB channels, increased bursting indicative of thalamocortical dysrhythmia or tinnitus-related increases in neurotransmitter availability/release onto postsynaptic sites (Kalappa et al., 2014; De Ridder et al., 2015; Elgoyhen et al., 2015; Caspary & Llano, 2017). 5) Columnar VIP neurons, thought to modulate PN excitability via disinhibition, showed tinnitus-related increases in excitability including reduction in resting membrane potential (depolarized state) and 6) tinnitus-related increases in rheobase current-evoked action potentials. Numbers of evoked action-potentials from VIP neurons were directly correlated with the severity of the tinnitus behavioral score. We hypothesize that tinnitus-related increases in VIP excitability results in inhibition of SOM and PV inhibitory interneurons, disinhibiting layer 5 PNs. Therefore, A1 VIP neurons may form an important link in our understanding of tinnitus-related maladaptive plastic changes within A1. Understanding the impact of tinnitus on the synaptic and intrinsic properties of A1 VIP neurons is important to better appreciate circuit changes underpinning tinnitus pathology. These same PN and VIP changes observed here have been previously detailed in a mouse model of neuropathic pain in the somatosensory cortex (Cichon et al., 2017). Collectively these findings suggest that tinnitus and chronic pain may share common cortical pathology.

The present findings are, in part, consistent with the maladaptive plasticity hypothesis of Turrigiano and colleagues, which details that activity deprivation induces homeostatic

changes in target neurons (Turrigiano et al., 1998). Noise-exposure used to induce tinnitus in the present study resulted in a permanent threshold shift at frequencies adjacent to the noise-exposure frequency. Accordingly, long-term sensory damage/deprivation is likely to initiate compensatory homeostatic mechanisms generally seen as increased spontaneous and driven activity, bursting and cross-connectivity in cochlear nucleus, inferior colliculus, auditory thalamus and auditory cortex (Brozoski et al., 2002; Bauer et al., 2008; Roberts et al., 2010; Noreña & Farley, 2013; Sedley, 2019; Shore & Wu, 2019; Henton & Tzounopoulos, 2021; Zhai et al., 2021; McGill et al., 2022).

In A1, tinnitus-related increases in sEPSC frequency and decreases in sIPSC frequency impacted layer 5 PN excitability changes and were directly correlated with tinnitus severity in behaviorally measured tinnitus (Figs. 2, 4), while layer 5 PNs from ENT animals showed no change in excitatory input. Tinnitus-related changes in excitatory/inhibitory homeostasis are consistent with previously described tinnitus-related plastic changes in central auditory neurotransmission (Noreña & Farley, 2013; Auerbach et al., 2014). Layer 5 PNs provide excitatory feedback to the MGB and extra-lemniscal IC as well as local cortical circuits (Williamson & Polley, 2019; Kommajosyula et al., 2021; Lesicko & Geffen, 2022). Tinnitus-related increases in layer 5 excitability theoretically could increase neuronal excitation at these target structures, potentially initiating reciprocal extra-lemniscal feed-forward excitation to A1 (Syka & Popelá, 1984; Stebbings et al., 2014; Williamson & Polley, 2019; Blackwell et al., 2020).

Miyakawa and colleagues found tinnitus-related decreases in A1 levels of the GABA synthesizing enzyme, GAD₆₅ (Miyakawa et al., 2019). Consistent with the present findings, Yang and colleagues (2011) working in a mouse model of tinnitus, found that A1 layer 2/3 PNs showed tinnitus-related down-regulation of GABA synthesis accompanied by increases in sEPSCs and decrease in sIPSCs (Yang et al., 2011). In mouse, noise exposure-related losses of PV interneurons, responsible for feed-forward inhibition, were hypothesized to decrease GABA release onto PNs in A1 (Miyakawa et al., 2019). Here in the rat model, we observed a significant loss of PV neurons in layer 4 and no significant loss of PV neurons across other layers of A1 (Table 2) but found a significant tinnitus-related down-regulation of sIPSCs onto layer 5 PNs. A significant, and likely compensatory, increase in sEPSC frequency onto layer 5 PNs also correlated to the behavioral measure of tinnitus across groups (Fig. 2E). Changes in sIPSC or sEPSC frequency are believed to reflect changes in input neurons activity. While amplitude changes are generally considered to reflect both postsynaptic changes and changes in neurotransmitter release from the input neurons (Bruns & Jahn, 1995). Tinnitus-related increases in sEPSC frequency suggested that the layer 5 PNs are receiving a greater level of excitatory input from excitatory connections within cortex: cortico-cortical, A1 columnar or non-A1 (Kalappa et al., 2014; De Ridder et al., 2015; Elgoyhen et al., 2015). Optogenetic stimulation of thalamocortical terminals evoked significantly larger EPSCs from ENT animals, which could reflect increased glutamate vesicular release, upregulation of AMPA/NMDA receptors or simply reflect tinnitus-related losses of PN inhibitory input (Murthy et al., 2001; Yang et al., 2011; De Ridder et al., 2015). A significantly larger portion of the thalamocortical EPSCs was mediated via polysynaptic mechanisms as the evoked EPSCs consisted of multiple peaks resembling polysynaptic

latencies, which in part, supported tinnitus-related increases in excitability throughout A1 layers (Fig. 3C) (Slater et al., 2019).

A1 layer 5 microcircuitry involves several types of excitatory pyramidal neurons and at least 4 different types of inhibitory interneurons. Layer 5 PNs receive local inhibitory input from nearby interneurons, primarily from PV and SOM interneurons, known to regulate their excitability (Letzkus et al., 2011; Mesik et al., 2015; Askew et al., 2019). Findings in present studies show tinnitus-related losses of pre- and postsynaptic GABAergic inhibition onto layer 5 PNs, consistent with the studies in layer 2/3 of A1 by Miyakawa and colleagues (Miyakawa et al., 2019). Similar to findings in a neuropathic pain model, A1 layer 5 neurons were found to receive significantly lower levels of inhibition as a result of tinnitus-related plastic changes of normal PV and SOM function (Fig. 4F, G) (Cichon et al., 2017). VIP neurons from ET animals showed a significant increase in the numbers of action potentials evoked by depolarizing electrical stimulation which directly correlated to the animal's tinnitus score. This VIP hyperexcitability was in part due to the tinnitus-related depolarized RMP likely again reflecting decreased endogenous levels of GABA (Fig. 7D). Activation of VIP neurons is known to inhibit the activity of PV and SOM inhibitory interneurons, resulting in decreased GABA_AR mediated tonic and phasic inhibition at the level of layer 5 PNs (Letzkus et al., 2011; Mesik et al., 2015; Cichon et al., 2017; Askew et al., 2019). Tinnitus-related increased excitability of VIP neurons would underpin the observed decreased feedforward inhibition via PV and SOM neurons, likely depolarizing layer 5 PNs (Fig. 2B) and similar to what was seen in somatosensory cortex by Cichon et al. (2017).

We found that PNs from ET animals were less sensitive to puff-applied GABA producing smaller amplitude/peak IPSCs and suggesting a significant loss of postsynaptic GABA_AR function. Previously described tinnitus-related loss of GAD₆₅ suggests decreased GABA synthesis, which has been shown to alter GABA_AR number and/or GABA_AR pharmacology via subunit switching (Wafford et al., 1993; Murthy et al., 2001). Extrasynaptic $\alpha_4\beta_2\delta$ -containing GABA_ARs are present in the neocortex and mediate robust non-desensitizing tonic inhibition (Drasbek & Jensen, 2005; Caspary & Llano, 2017). The observed tinnitus-related loss of tonic GABA_AR current was likely due to a loss of ambient GABA, since the present patch-clamp and receptor binding studies found no significant tinnitus-related changes suggestive of a loss in extrasynaptic GABA_AR number (Fig. 6C–E).

Tinnitus not only affects the auditory pathways, it also affects various attentional and limbic/emotional systems (Kraus & Canlon, 2012; Chen et al., 2017; Besteher et al., 2019). A1 layer 5 PNs recorded in the present study may make multiple excitatory connections to subcortical centers such as IC, MGB, amygdala or intra-cortical targets (Asokan et al., 2018; Baker et al., 2018). Increased activity of layer 5 PNs may worsen tinnitus pathology by various mechanisms including facilitation of: 1) the activity of trauma-associated limbic regions; 2) the pathological reverberant feedback loop or pathological synchrony between IC, MGB and A1; and 3) amplifying cortical responses to sub-perceptual inputs, and/or combinations of all these possibilities.

In conclusion, in an established tinnitus model, the present study describes tinnitus-related pre- and postsynaptic changes in the physiology of A1 layer 5 pyramidal and VIP neurons from ET animals but not from ENT rat A1. Tinnitus-related increases in excitability of layer 5 PNs were accompanied by increased excitability of VIP interneurons. Future studies will examine tinnitus-related changes in PV and SOM inhibitory interneurons while considering pharmacologic agents targeting VIP excitability.

Supplementary Material

Refer to Web version on PubMed Central for supplementary material.

Acknowledgement

This work was supported by Department of Defense Award PR180160 to DMC, NIH DC015388 to TAH, and NIH DC016599 and DC013073 to DAL. We thank Dr. Thomas Brozoski, Dr. Brandon Cox, and Kurt Wisner for assistance with the animal model and Dr. Benjamin Richardson for sharing his knowledge of electrophysiological data analysis.

Biography



Madan Ghimire completed his doctorate under the mentorship of Dr. Donald Caspary at Southern Illinois University School of Medicine, Department of Pharmacology and Neuroscience. His doctoral research focused to understand the tinnitus-related disruption in physiological and cholinergic function in layer 5 pyramidal neurons and VIP neurons of the primary auditory cortex. Currently, he is a post-doctoral associate in the Department of Otolaryngology at University of Pittsburgh under mentorship of Dr. Ross Williamson, where he is working to understand the role of projection neurons of primary auditory cortex in stimulus encoding.

Data availability statement

All data supporting the results have been included in the manuscript and figures. Additional data in support of the findings of this study are available from the corresponding author, upon request.

References

- Askew CE, Lopez AJ, Wood MA & Metherate R. (2019). Nicotine excites VIP interneurons to disinhibit pyramidal neurons in auditory cortex. *Synapse* 73, e22116. [PubMed: 31081950]
- Asokan MM, Williamson RS, Hancock KE & Polley DB. (2018). Sensory overamplification in layer 5 auditory corticofugal projection neurons following cochlear nerve synaptic damage. *Nature Communications* 9, 2468.
- Auerbach BD, Rodrigues PV & Salvi RJ. (2014). Central Gain Control in Tinnitus and Hyperacusis. *Frontiers in Neurology* 5.

- Baker A, Kalmbach B, Morishima M, Kim J, Juavinett A, Li N & Dembrow N. (2018). Specialized Subpopulations of Deep-Layer Pyramidal Neurons in the Neocortex: Bridging Cellular Properties to Functional Consequences. *The Journal of Neuroscience* 38, 5441–5455. [PubMed: 29798890]
- Banks MI & Smith PH. (2011). Thalamocortical Relations. In *The Auditory Cortex*, ed. Winer JA & Schreiner CE, pp. 75–97. Springer US, Boston, MA.
- Barbour DL & Callaway EM. (2008). Excitatory Local Connections of Superficial Neurons in Rat Auditory Cortex. *The Journal of Neuroscience* 28, 11174–11185. [PubMed: 18971460]
- Bauer CA & Brozoski TJ. (2001). Assessing tinnitus and prospective tinnitus therapeutics using a psychophysical animal model. *J Assoc Res Otolaryngol* 2, 54–64. [PubMed: 11545150]
- Bauer CA, Turner JG, Caspary DM, Myers KS & Brozoski TJ. (2008). Tinnitus and inferior colliculus activity in chinchillas related to three distinct patterns of cochlear trauma. *Journal of Neuroscience Research* 86, 2564–2578. [PubMed: 18438941]
- Belelli D, Harrison NL, Maguire J, Macdonald RL, Walker MC & Cope DW. (2009). Extrasynaptic GABA_A Receptors: Form, Pharmacology, and Function. *The Journal of Neuroscience* 29, 12757–12763. [PubMed: 19828786]
- Besteher B, Gaser C, Ivanšić D, Guntinas-Lichius O, Döbel C & Nenadić I. (2019). Chronic tinnitus and the limbic system: Reappraising brain structural effects of distress and affective symptoms. *NeuroImage: Clinical* 24, 101976. [PubMed: 31494400]
- Blackwell J & Geffen M. (2017). Progress and challenges for understanding the function of cortical microcircuits in auditory processing. *Nature Communications* 8.
- Blackwell JM, Lesicko AMH, Rao W, De Biasi M & Geffen MN. (2020). Auditory cortex shapes sound responses in the inferior colliculus. *eLife* 9, e51890. [PubMed: 32003747]
- Boudkazi S, Carlier E, Ankri N, Caillard O, Giraud P, Fronzaroli-Molinieres L & Debanne D. (2007). Release-dependent variations in synaptic latency: a putative code for short-and long-term synaptic dynamics. *Neuron* 56, 1048–1060. [PubMed: 18093526]
- Brozoski TJ & Bauer CA. (2005). The effect of dorsal cochlear nucleus ablation on tinnitus in rats. *Hear Res* 206, 227–236. [PubMed: 16081010]
- Brozoski TJ, Bauer CA & Caspary DM. (2002). Elevated Fusiform Cell Activity in the Dorsal Cochlear Nucleus of Chinchillas with Psychophysical Evidence of Tinnitus. *The Journal of Neuroscience* 22, 2383–2390. [PubMed: 11896177]
- Bruns D & Jahn R. (1995). Real-time measurement of transmitter release from single synaptic vesicles. *Nature* 377, 62–65. [PubMed: 7659162]
- Caspary DM & Llano DA. (2017). Auditory thalamic circuits and GABA_A receptor function: Putative mechanisms in tinnitus pathology. *Hearing Research* 349, 197–207. [PubMed: 27553899]
- Chen Y-C, Xia W, Chen H, Feng Y, Xu J-J, Gu J-P, Salvi R & Yin X. (2017). Tinnitus distress is linked to enhanced resting-state functional connectivity from the limbic system to the auditory cortex. *Human Brain Mapping* 38, 2384–2397. [PubMed: 28112466]
- Cichon J, Blanck TJJ, Gan W-B & Yang G. (2017). Activation of cortical somatostatin interneurons prevents the development of neuropathic pain. *Nature Neuroscience* 20, 1122–1132. [PubMed: 28671692]
- De Ridder D, Vanneste S, Langguth B & Llinas R. (2015). Thalamocortical Dysrhythmia: A Theoretical Update in Tinnitus. *Frontiers in neurology* 6, 124. [PubMed: 26106362]
- Deng D, Masri S, Yao L, Ma X, Cao X, Yang S, Bao S & Zhou Q. (2020). Increasing endogenous activity of NMDARs on GABAergic neurons increases inhibition, alters sensory processing and prevents noise-induced tinnitus. *Scientific Reports* 10, 11969. [PubMed: 32686710]
- Drasbek KR & Jensen K. (2005). THIP, a Hypnotic and Antinociceptive Drug, Enhances an Extrasynaptic GABA_A Receptor-mediated Conductance in Mouse Neocortex. *Cerebral Cortex* 16, 1134–1141. [PubMed: 16221925]
- Eggermont JJ. (2013). Hearing loss, hyperacusis, or tinnitus: What is modeled in animal research? *Hearing Research* 295, 140–149. [PubMed: 22330978]
- Elgoyhen AB, Langguth B, De Ridder D & Vanneste S. (2015). Tinnitus: perspectives from human neuroimaging. *Nature Reviews Neuroscience* 16, 632–642. [PubMed: 26373470]
- Geven LI, de Kleine E, Willemsen ATM & van Dijk P. (2014). Asymmetry in primary auditory cortex activity in tinnitus patients and controls. *Neuroscience* 256, 117–125. [PubMed: 24161276]

- Ghimire M, Cai R, Ling L, Hackett TA & Caspary DM. (2020). Nicotinic Receptor Subunit Distribution in Auditory Cortex: Impact of Aging on Receptor Number and Function. *J Neurosci* 40, 5724–5739. [PubMed: 32541068]
- Gil Z & Amitai Y. (1996). Properties of convergent thalamocortical and intracortical synaptic potentials in single neurons of neocortex. *Journal of Neuroscience* 16, 6567–6578. [PubMed: 8815933]
- Gonchar Y, Wang Q & Burkhalter A. (2008). Multiple distinct subtypes of GABAergic neurons in mouse visual cortex identified by triple immunostaining. *Frontiers in Neuroanatomy* 2.
- Henton A & Tzounopoulos T. (2021). What’s the buzz? The neuroscience and the treatment of tinnitus. *Physiological Reviews* 101, 1609–1632. [PubMed: 33769102]
- Huang CL & Winer JA. (2000). Auditory thalamocortical projections in the cat: Laminar and areal patterns of input. *Journal of Comparative Neurology* 427, 302–331. [PubMed: 11054695]
- Kalappa BI, Brozski TJ, Turner JG & Caspary DM. (2014). Single unit hyperactivity and bursting in the auditory thalamus of awake rats directly correlates with behavioural evidence of tinnitus. *The Journal of physiology* 592, 5065–5078. [PubMed: 25217380]
- Kaltenbach JA. (2011). Tinnitus: Models and mechanisms. *Hearing Research* 276, 52–60. [PubMed: 21146597]
- Kaltenbach JA, Zacharek MA, Zhang J & Frederick S. (2004). Activity in the dorsal cochlear nucleus of hamsters previously tested for tinnitus following intense tone exposure. *Neuroscience Letters* 355, 121–125. [PubMed: 14729250]
- Kaltenbach JA, Zhang J & Finlayson P. (2005). Tinnitus as a plastic phenomenon and its possible neural underpinnings in the dorsal cochlear nucleus. *Hearing Research* 206, 200–226. [PubMed: 16081009]
- Kommajosyula SP, Bartlett EL, Cai R, Ling L & Caspary DM. (2021). Corticothalamic projections deliver enhanced responses to medial geniculate body as a function of the temporal reliability of the stimulus. *The Journal of Physiology* 599, 5465–5484. [PubMed: 34783016]
- Kraus KS & Canlon B. (2012). Neuronal connectivity and interactions between the auditory and limbic systems. Effects of noise and tinnitus. *Hearing Research* 288, 34–46. [PubMed: 22440225]
- Kujawa SG & Liberman MC. (2009). Adding Insult to Injury: Cochlear Nerve Degeneration after “Temporary” Noise-Induced Hearing Loss. *The Journal of Neuroscience* 29, 14077–14085. [PubMed: 19906956]
- Lesicko AM & Geffen MN. (2022). Diverse functions of the auditory cortico-collicular pathway. *Hearing Research*, 108488. [PubMed: 35351323]
- Letzkus JJ, Wolff SBE, Meyer EMM, Tovote P, Courtin J, Herry C & Lüthi A. (2011). A disinhibitory microcircuit for associative fear learning in the auditory cortex. *Nature* 480, 331–335. [PubMed: 22158104]
- Ling L & Caspary D. (2013). Autoradiographic 3H-Gaboxadol Receptor Binding Protocol. *Bio-protocol* 3.
- Liu C, Xu T, Liu X, Huang Y, Wang H, Luo B & Sun J. (2018). Acoustic Trauma Changes the Parvalbumin-Positive Neurons in Rat Auditory Cortex. *Neural Plasticity* 2018, 9828070. [PubMed: 29593786]
- Llano DA, Turner J & Caspary DM. (2012). Diminished cortical inhibition in an aging mouse model of chronic tinnitus. *J Neurosci* 32, 16141–16148. [PubMed: 23152598]
- Ma W-LD, Hidaka H & May BJ. (2006). Spontaneous activity in the inferior colliculus of CBA/J mice after manipulations that induce tinnitus. *Hearing Research* 212, 9–21. [PubMed: 16307852]
- McGill M, Hight AE, Watanabe YL, Parthasarathy A, Cai D, Clayton K, Hancock KE, Takesian A, Kujawa SG & Polley DB. (2022). Neural signatures of auditory hypersensitivity following acoustic trauma. *Elife* 11, e80015. [PubMed: 36111669]
- Mesik L, Ma W-p, Li L-y, Ibrahim LA, Huang ZJ, Zhang LI & Tao HW. (2015). Functional response properties of VIP-expressing inhibitory neurons in mouse visual and auditory cortex. *Frontiers in Neural Circuits* 9.
- Miyakawa A, Wang W, Cho S-J, Li D, Yang S & Bao S. (2019). Tinnitus Correlates with Downregulation of Cortical Glutamate Decarboxylase 65 Expression But Not Auditory Cortical Map Reorganization. *The Journal of Neuroscience* 39, 9989–10001. [PubMed: 31704784]

- Murthy VN, Schikorski T, Stevens CF & Zhu Y. (2001). Inactivity Produces Increases in Neurotransmitter Release and Synapse Size. *Neuron* 32, 673–682. [PubMed: 11719207]
- Nelson A, Schneider DM, Takatoh J, Sakurai K, Wang F & Mooney R. (2013). A Circuit for Motor Cortical Modulation of Auditory Cortical Activity. *The Journal of Neuroscience* 33, 14342–14353. [PubMed: 24005287]
- Nguyen A, Khaleel HM & Razak KA. (2017). Effects of noise-induced hearing loss on parvalbumin and perineuronal net expression in the mouse primary auditory cortex. *Hearing research* 350, 82–90. [PubMed: 28460252]
- Noreña AJ. (2011). An integrative model of tinnitus based on a central gain controlling neural sensitivity. *Neuroscience & Biobehavioral Reviews* 35, 1089–1109. [PubMed: 21094182]
- Noreña AJ & Farley BJ. (2013). Tinnitus-related neural activity: Theories of generation, propagation, and centralization. *Hearing research* 295, 161–171. [PubMed: 23088832]
- Paxinos G & Watson C. (1998). A stereotaxic atlas of the rat brain. New York: Academic.
- Pfeffer CK, Xue M, He M, Huang ZJ & Scanziani M. (2013). Inhibition of inhibition in visual cortex: the logic of connections between molecularly distinct interneurons. *Nature neuroscience* 16, 1068–1076. [PubMed: 23817549]
- Phillips EAK, Schreiner CE & Hasenstaub AR. (2017). Cortical Interneurons Differentially Regulate the Effects of Acoustic Context. *Cell Reports* 20, 771–778. [PubMed: 28746863]
- Pi H-J, Hangya B, Kvitsiani D, Sanders JI, Huang ZJ & Kepecs A. (2013). Cortical interneurons that specialize in disinhibitory control. *Nature* 503, 521–524. [PubMed: 24097352]
- Richardson BD, Brozoski TJ, Ling LL & Caspary DM. (2012). Targeting inhibitory neurotransmission in tinnitus. *Brain Research* 1485, 77–87. [PubMed: 22405692]
- Richardson BD, Ling LL, Uteshev VV & Caspary DM. (2011). Extrasynaptic GABAA receptors and tonic inhibition in rat auditory thalamus. *PloS one* 6, e16508. [PubMed: 21298071]
- Richardson BD, Ling LL, Uteshev VV & Caspary DM. (2013). Reduced GABA_A Receptor-Mediated Tonic Inhibition in Aged Rat Auditory Thalamus. *The Journal of Neuroscience* 33, 1218–1227. [PubMed: 23325258]
- Roberts LE, Eggermont JJ, Caspary DM, Shore SE, Melcher JR & Kaltenbach JA. (2010). Ringing Ears: The Neuroscience of Tinnitus. *The Journal of Neuroscience* 30, 14972–14979. [PubMed: 21068300]
- Ropp T-JF, Tiedemann KL, Young ED & May BJ. (2014). Effects of Unilateral Acoustic Trauma on Tinnitus-Related Spontaneous Activity in the Inferior Colliculus. *Journal of the Association for Research in Otolaryngology* 15, 1007–1022. [PubMed: 25255865]
- Sametsky EA, Turner JG, Larsen D, Ling L & Caspary DM. (2015). Enhanced GABA-A-Mediated Tonic Inhibition in Auditory Thalamus of Rats with Behavioral Evidence of Tinnitus. *The Journal of Neuroscience* 35, 9369–9380. [PubMed: 26109660]
- Schaette R & Kempter R. (2006). Development of tinnitus-related neuronal hyperactivity through homeostatic plasticity after hearing loss: a computational model. *European Journal of Neuroscience* 23, 3124–3138. [PubMed: 16820003]
- Schneider DM, Nelson A & Mooney R. (2014). A synaptic and circuit basis for corollary discharge in the auditory cortex. *Nature* 513, 189–194. [PubMed: 25162524]
- Schofield CM & Huguenard JR. (2007). GABA Affinity Shapes IPSCs in Thalamic Nuclei. *The Journal of Neuroscience* 27, 7954–7962. [PubMed: 17652586]
- Sedley W. (2019). Tinnitus: Does Gain Explain? *Neuroscience* 407, 213–228. [PubMed: 30690137]
- Sedley W, Parikh J, Edden RAE, Tait V, Blamire A & Griffiths TD. (2015). Human Auditory Cortex Neurochemistry Reflects the Presence and Severity of Tinnitus. *The Journal of Neuroscience* 35, 14822–14828. [PubMed: 26538652]
- Shore SE & Wu C. (2019). Mechanisms of Noise-Induced Tinnitus: Insights from Cellular Studies. *Neuron* 103, 8–20. [PubMed: 31271756]
- Slater BJ, Sons SK, Yuditsev G, Lee CM & Llano DA. (2019). Thalamocortical and Intracortical Inputs Differentiate Layer-Specific Mouse Auditory Corticocollicular Neurons. *The Journal of Neuroscience* 39, 256–270. [PubMed: 30361396]

- Sottile SY, Hackett TA, Cai R, Ling L, Llano DA & Caspary DM. (2017). Presynaptic Neuronal Nicotinic Receptors Differentially Shape Select Inputs to Auditory Thalamus and Are Negatively Impacted by Aging. *The Journal of Neuroscience* 37, 11377–11389. [PubMed: 29061702]
- Stebbins KA, Lesicko AMH & Llano DA. (2014). The auditory corticocollicular system: Molecular and circuit-level considerations. *Hearing Research* 314, 51–59. [PubMed: 24911237]
- Syka J & Popelá J. (1984). Inferior colliculus in the rat: Neuronal responses to stimulation of the auditory cortex. *Neuroscience Letters* 51, 235–240. [PubMed: 6514239]
- Takesian AE, Bogart LJ, Lichtman JW & Hensch TK. (2018). Inhibitory circuit gating of auditory critical-period plasticity. *Nature neuroscience* 21, 218–227. [PubMed: 29358666]
- Turrigiano GG, Leslie KR, Desai NS, Rutherford LC & Nelson SB. (1998). Activity-dependent scaling of quantal amplitude in neocortical neurons. *Nature* 391, 892–896. [PubMed: 9495341]
- Wafford K, Whiting P & Kemp J. (1993). Differences in affinity and efficacy of benzodiazepine receptor ligands at recombinant gamma-aminobutyric acidA receptor subtypes. *Molecular Pharmacology* 43, 240–244. [PubMed: 8381510]
- Wang H, Brozoski TJ, Turner JG, Ling L, Parrish JL, Hughes LF & Caspary DM. (2009). Plasticity at glycinergic synapses in dorsal cochlear nucleus of rats with behavioral evidence of tinnitus. *Neuroscience* 164, 747–759. [PubMed: 19699270]
- Williamson RS & Polley DB. (2019). Parallel pathways for sound processing and functional connectivity among layer 5 and 6 auditory corticofugal neurons. *eLife* 8.
- Winer JA & Lee CC. (2007). The distributed auditory cortex. *Hearing Research* 229, 3–13. [PubMed: 17329049]
- Yang S, Weiner BD, Zhang LS, Cho SJ & Bao S. (2011). Homeostatic plasticity drives tinnitus perception in an animal model. *Proc Natl Acad Sci U S A* 108, 14974–14979. [PubMed: 21896771]
- Zhai T, Ash-Rafzadeh A, Hu X, Kim J, San Juan JD, Filipiak C, Guo K, Islam MN, Kovelman I & Basura GJ. (2021). Tinnitus and auditory cortex; Using adapted functional near-infrared-spectroscopy to expand brain imaging in humans. *Laryngoscope Investigative Otolaryngology* 6, 137–144. [PubMed: 33614942]
- Zhang J. (2013). Auditory cortex stimulation to suppress tinnitus: Mechanisms and strategies. *Hearing research* 295, 38–57. [PubMed: 22683861]

Key points:

- Identify tinnitus-related changes in synaptic function of specific neuronal subtypes in a reliable animal model of tinnitus.
- Findings show direct and indirect tinnitus-related losses of normal inhibitory function at A1 layer 5 pyramidal cells, and increased VIP excitability.
- Findings are similar to what has been shown for neuropathic pain suggesting that restoring normal inhibitory function at synaptic inputs onto A1 pyramidal neurons could conceptually reduce tinnitus discomfort.

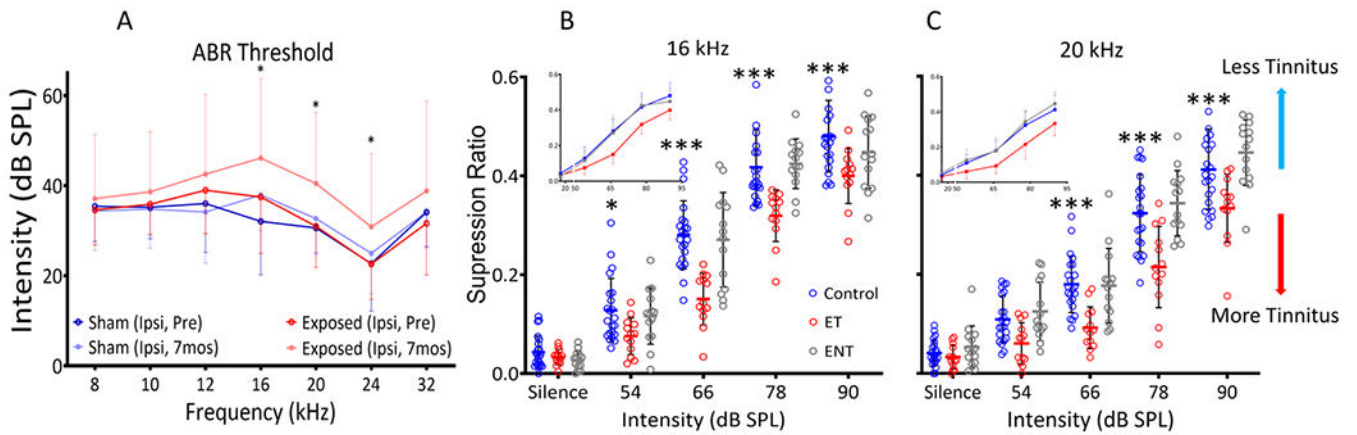


Figure 1: Animal model of tinnitus.

A. ABR threshold before and after unilateral noise-exposure in sham exposed controls ($n = 40$) and noise-exposed animals ($n = 24$). A modest significant shift in ABR threshold after noise-exposure was observed ($F(1, 554) = 25.28, p = 0.0001$, Two-way ANOVA). B, C. Based on their suppression ratios, animals trained on the discrimination task were categorized as Control (Ctrl, $n = 22$), exposed tinnitus (ET, $n = 15$) and exposed non-tinnitus (ENT, $n = 13$). The same data is plotted as a simple line plot (small graph) and for each individual rat from the three groups. A significant separation between the suppression ratios of Control and ET was observed at 16 kHz (B) ($F(2, 230) = 32.28, p < 0.0001$, Bonferroni post-hoc test) and 20 kHz (C) ($F(2, 230) = 35.77, p < 0.0001$, Bonferroni post-hoc test) frequency tests. All results are plotted as mean \pm SD. * $p < 0.05$, *** $p < 0.001$.

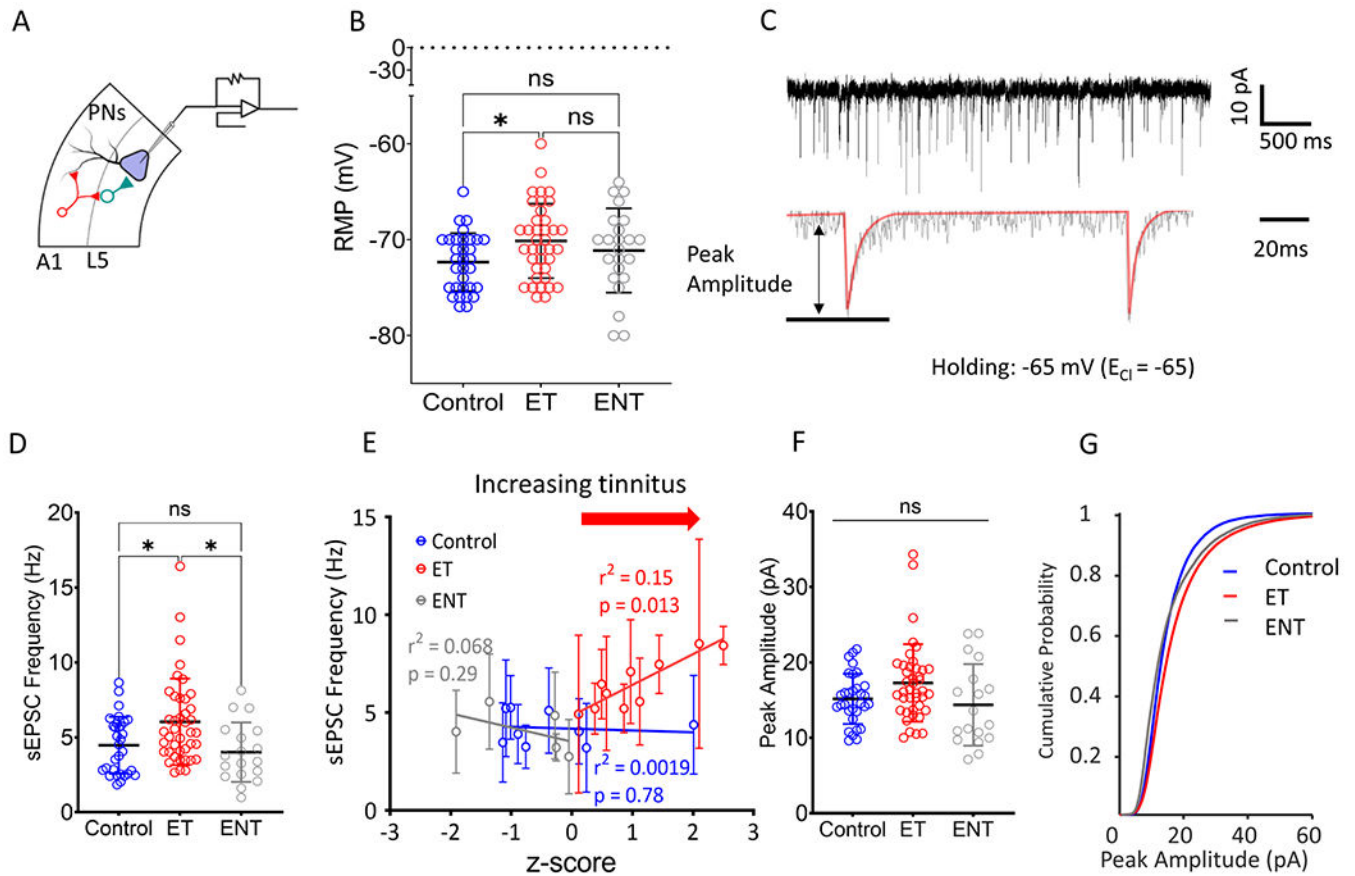


Figure 2: Tinnitus-related increases in activity of excitatory input neurons onto layer 5 PN.

A. Illustration representing patch-clamp recording configuration from A1 layer 5 PN. B. Resting membrane potential (RMP) of PN from ET animals was depolarized relative to layer 5 PN from control neurons (Control, Mean \pm SD mV, -72.34 ± 3.02 , $n = 32$; ET, -70.16 ± 3.85 , $n = 38$; ENT, -71.13 ± 4.39 , $n = 23$; $F(2, 90) = 2.96$, $p = 0.0336$, One-way ANOVA with Bonferroni post-hoc test). C. Top, exemplar recording trace of continuous voltage-clamped sEPSC recordings, bottom, measurement of peak amplitude. D. Tinnitus-related increase in frequency of sEPSCs recorded from layer 5 PN from ET animals (Control, Mean \pm SD Hz, 4.47 ± 1.89 , $n = 31$; ET 6.032 ± 2.88 , $n = 41$; ENT, 4.007 ± 1.98 , $n = 18$, $F(2, 87) = 5.38$, $p = 0.0038$; $p = 0.024$ Control vs ET and $p = 0.011$, ET vs ENT, One-way ANOVA with Bonferroni post-hoc test). E. Simple linear regression analysis was performed to predict sEPSC frequency based on normalized tinnitus score(z-score) (Control, $F(1,38) = 0.07$, $r^2 = 0.0019$, $p = 0.78$; ET, $F(1,38) = 6.79$, $r^2 = 0.15$, $p = 0.013$; ENT, $F(1, 16) = 1.18$, $r^2 = 0.068$, $p = 0.29$). F. Amplitude of sEPSCs recorded from layer 5 PN in control ET and ENT animals (Control, Mean \pm SD pA, 15.17 ± 3.32 , $n = 31$; ET, 17.27 ± 5.13 , $n = 41$; ENT, 14.37 ± 5.41 , $n = 4$, $F(2, 87) = 3.14$, $p = 0.048$, One-way ANOVA). G. Cumulative curves of sEPSC amplitude. * $p < 0.05$. See methods for z-score normalization.

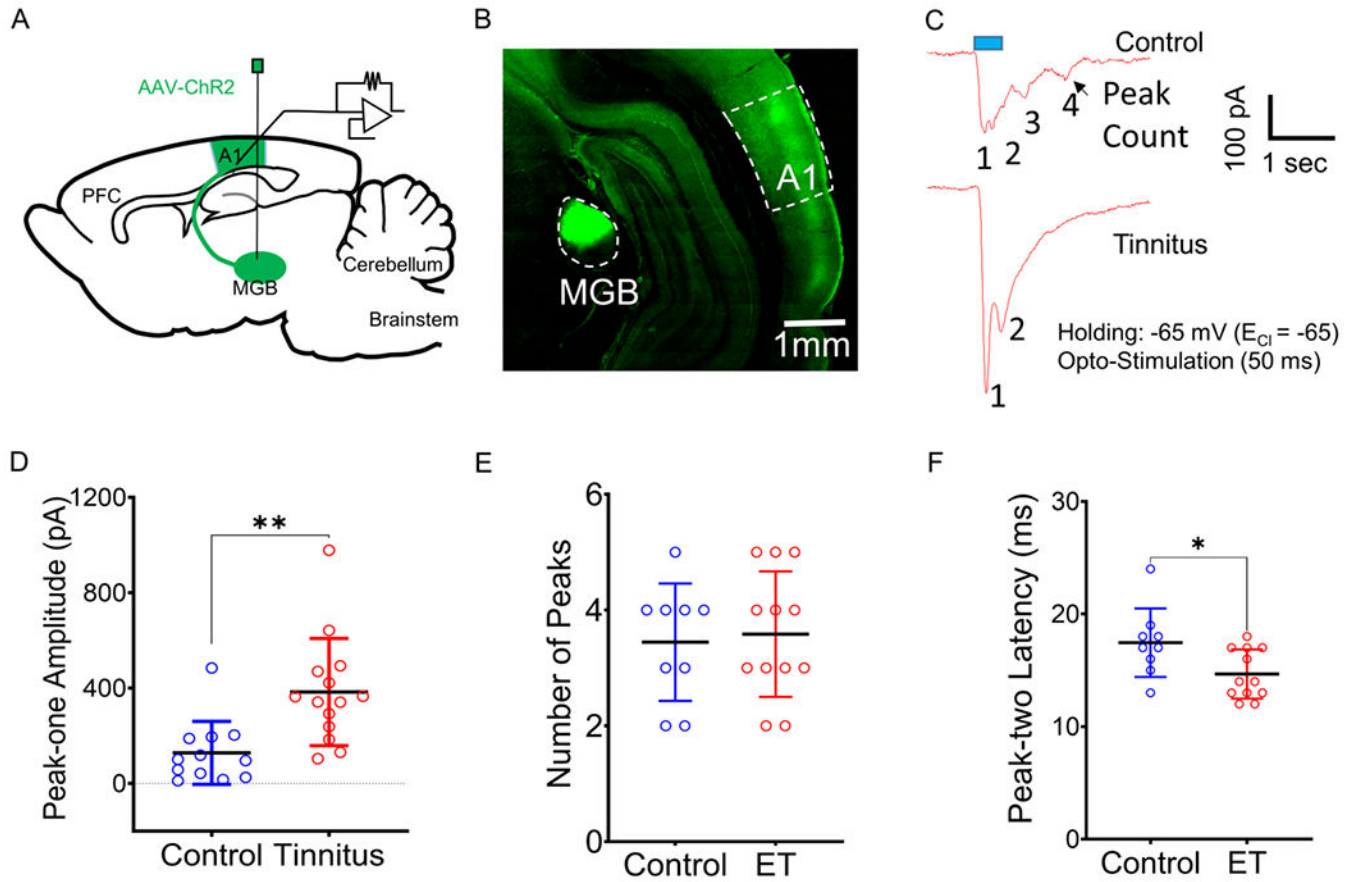


Figure 3: ET animals show increased thalamocortical excitability.

A. Illustration showing injection of AAV-ChR2 in the MGB of control and ET animals. B. MGB principal projections into layers 1 and 4 of A1. C. Exemplar traces from control and ET PN showing multi-peaked optically evoked EPSCs from layer 5 PN evoked by stimulation of MGB terminals. D. Peak-one amplitude of evoked sEPSC from layer 5 PN (Control, Baseline, Mean \pm SD pA, 128.3 ± 132 , $n = 12$; Tinnitus, 383 ± 224 , $n = 14$, $t(24) = 3.44$, $p = 0.002$, t -test). E. Number of EPSC peaks evoked with 50 ms optical stimulation of thalamocortical terminals (Control, Baseline, Mean \pm SD, 3.44 ± 1.01 , $n = 9$; Tinnitus, 3.58 ± 1.08 , $n = 12$) and F. Peak-two latency (Control, Baseline, Mean \pm SD ms, 17.44 ± 3.04 , $n = 9$; Tinnitus, 14.67 ± 2.18 , $n = 12$, $t(19) = 2.43$, $p = 0.024$, t -test). * $p < 0.05$, ** < 0.01 .

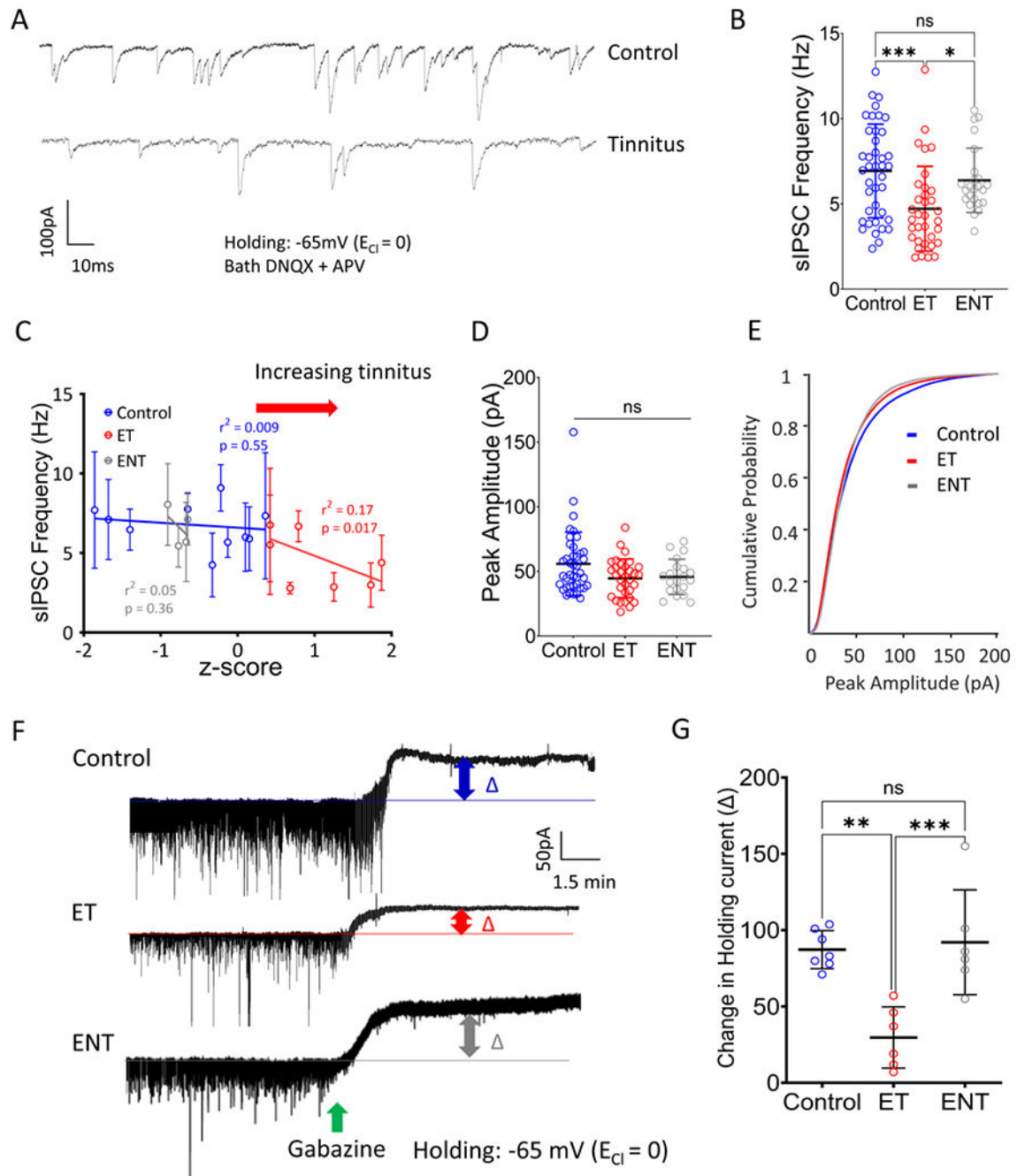


Figure 4: Tinnitus-related loss of GABAergic input onto layer 5 PNs.

A. Exemplar traces of sIPSCs recorded from layer 5 PNs from control (top) and tinnitus (bottom) animals. B. Decreased frequency of sIPSCs recorded from layer 5 PNs from control, ET and ENT animals (Control, Mean \pm SD Hz, 6.93 ± 2.74 , $n = 40$; ET, 4.71 ± 2.48 , $n = 34$; ENT, 6.58 ± 2.33 , $n = 21$, $F(2,92) = 7.4$, $p = 0.001$; $p = 0.0011$ control vs ET, $p = 0.9$ control vs ENT, and $p = 0.038$ ET vs ENT, One-way ANOVA with Bonferroni post-hoc test). C. Plot of sIPSC frequency from layer 5 PNs in control, ET and ENT rats against their normalized tinnitus scores (z-score) (Control, $F(1, 39) = 0.35$, $p = 0.55$, r^2

= 0.009; ET, $F(1, 30) = 6.29$, $p = 0.01$, $r^2 = 0.17$; ENT, $F(1, 16) = 0.88$, $p = 0.36$, $r^2 = 0.05$). D. No tinnitus-related changes in average peak amplitude of sIPSCs from layer 5 PNs from control vs ET animals (Control, Mean \pm SD pA, 55.82 ± 24.46 , $n = 40$; ET, 44.6 ± 14.88 , $n = 32$; ENT, 45.72 ± 13.62 , $n = 20$, $F(2, 89) = 3.49$, $p = 0.03$; $p = 0.0513$ control vs ET, $p = 0.18$ control vs ENT, and $p = 0.9$, ET vs ENT, One-way ANOVA with Bonferroni post-hoc test). E. Cumulative probability plot of sIPSC amplitude. F. Exemplar traces showing tinnitus-related changes in GABA_AR mediated tonic current in layer 5 PNs from control (top) and tinnitus (bottom) animals are revealed following bath application of 40 μ M gabazine. G. Quantification of tonic current (Control, Mean \pm SD pA, 87.23 ± 12.43 , $n = 7$; ET, 29.67 ± 20.04 , $n = 6$; ENT, 92.00 ± 34.35 , $n = 6$, $F(2, 16) = 13.34$, $p = 0.0004$; $p = 0.0013$ control vs ET, $p = 0.9$ control vs ENT, and $p = 0.0009$ ET vs ENT, One-way ANOVA with Bonferroni post-hoc). * $p < 0.05$, ** < 0.01 , *** < 0.001 . See methods for z-score normalization.

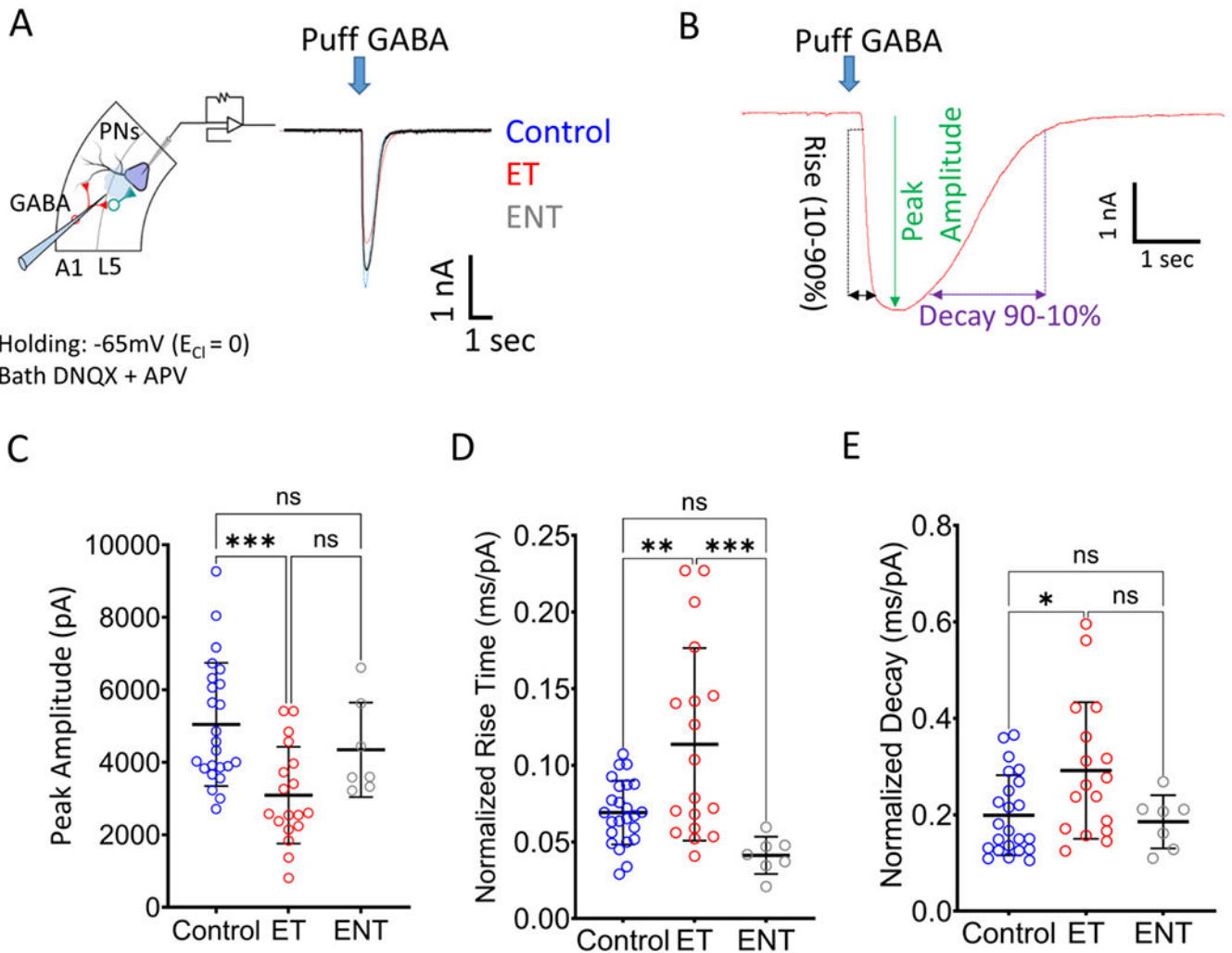


Figure 5: Tinnitus-related disruption in GABA_A receptor pharmacokinetics in layer 5 PN.

A. Illustration showing whole-cell patch-clamp recordings from layer 5 PN while puffing GABA (left); exemplar traces (right) in response to 20ms puffed GABA onto layer 5 PN from control (Blue), ET (red) and ENT (gray) rats. B. Measurements of evoked current in response to 20ms puffed GABA, peak amplitude (green), rise time (black) and decay time (purple). C. Tinnitus-related reduction in peak amplitude of evoked current to puffed GABA in layer 5 PN (Control, Mean \pm SD pA, 5043 ± 1700 , $n = 24$; ET, 3153 ± 1708 , $n = 18$; ENT, 4343 ± 1305 , $n = 7$, $F(2, 46) = 8.44$, $p = 0.0008$; $p = 0.0003$ control vs ET, $p = 0.58$ control vs ENT, and $p = 0.21$ ET vs ENT, One-way ANOVA with Bonferroni post-hoc test). D. Tinnitus-related reduction in rise time normalized to peak amplitude in control and ET animals (Control, Mean \pm SD ms/pA, 0.069 ± 0.02 , $n = 24$; ET, 0.11 ± 0.06 , $n = 18$; ENT, 0.04 ± 0.012 , $n = 7$, $F(2, 46) = 9.92$, $p = 0.0003$; $p = 0.0023$ control vs ET, $p = 0.22$ control vs ENT, and $p = 0.0008$ ET vs ENT, One-way ANOVA with Bonferroni post-hoc test). E. Decay-time normalized to peak amplitude in control and ET animals (Control, Mean \pm SD ms/pA, 0.19 ± 0.08 , $n = 24$; ET, 0.28 ± 0.14 , $n = 18$; ENT, 0.18 ± 0.05 , $n = 7$, $F(1, 46) = 2.6$, $p = 0.016$; $p = 0.035$ control vs ET, $p = 0.9$ control vs ENT, and $p = 0.09$ ET vs ENT, One-way ANOVA with Bonferroni post-hoc test). * $p < 0.05$ **, < 0.01 , *** < 0.001 .

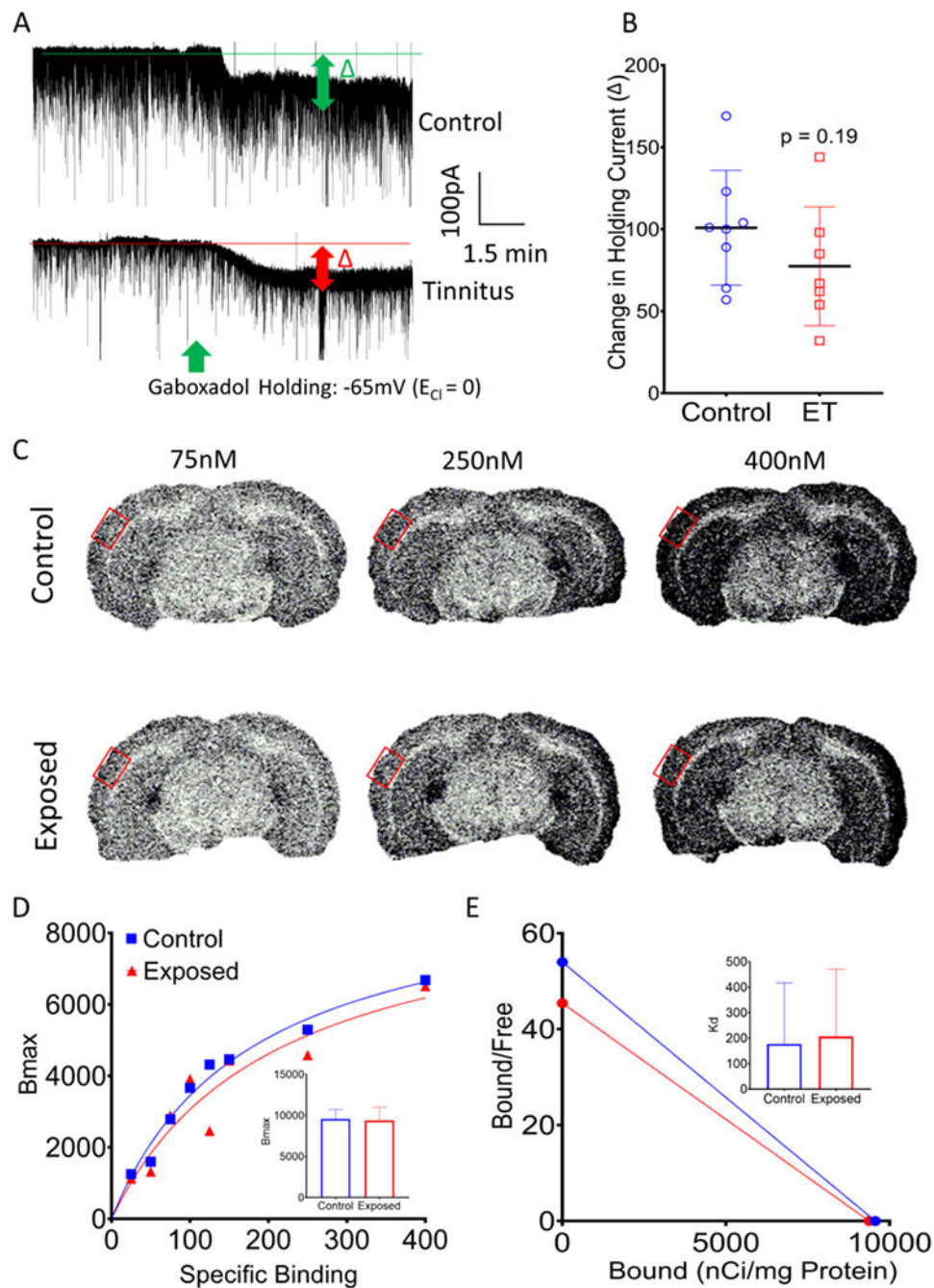


Figure 6: No extra-synaptic GABA_AR tinnitus-related change.

A. Exemplars showing extrasynaptic GABA_AR mediated tonic currents in whole-cell recordings. GABA_AR mediated tonic currents from layer 5 PNs of control (top) and tinnitus (bottom) animals following bath application of the selective agonist gaboxadol (GBX). B. Tinnitus-related changes in holding current in response to bath GBX (Control, Mean \pm SD pA, 100.9 ± 34.98 , $n = 8$ neurons, 2 animals; Tinnitus, 77.43 ± 34.11 , $n = 7$ neurons, 2 animals; $t(13) = 1.27$, $p = 0.19$, t -test). C. Exemplar autoradiographic images showing [³H]GBX binding in coronal brain sections containing A1 (red box) from control

(top) and similarly noise-exposed (bottom) animals at 75, 250 and 400 nM concentration. D. Saturation binding curves show maximum binding sites in the A1 in control vs noise-exposed animals (Control, Mean \pm SD nCi/mg protein, 9561 ± 1166 , $n = 30$ samples, 10 animals; Tinnitus, 9376 ± 1627 , $n = 15$ samples, 5 animals; $t(43) = 0.45$, $p = 0.66$, t -test). E. Calculation of dissociation constant (Kd) as a function of binding affinity show no noise-exposure related changes (Control, Mean \pm SD nM 177.1 ± 240.1 , $n = 30$ samples, 10 animals; Tinnitus, 206.4 ± 264.8 , $n = 15$ samples, 5 animals; $t(43) = 0.37$, $p = 0.71$, t -test).

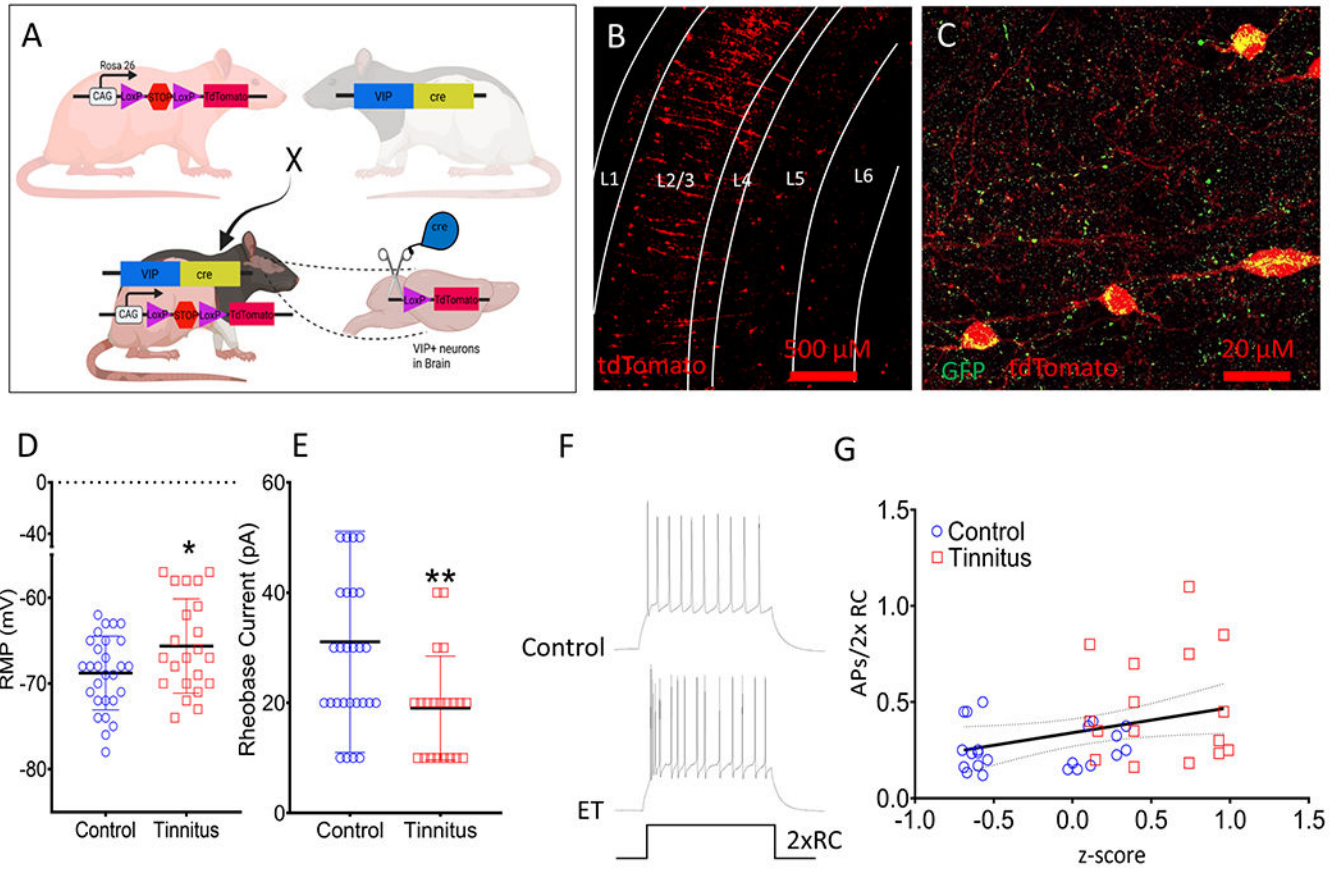


Figure 7: VIP neurons show tinnitus-related increased excitability.

A. Illustration showing the generation of $VIP^{Cre}:Rosa26^{tdTomato}$ rats by breeding VIP-Cre rats with tdTomato reporter rats. B, C. VIP x tdTomato rats express fluorescent tdTomato protein in VIP+ rats which was validated by using anti-VIP antibody in A1 slices. D. Tinnitus-related decrease in VIP neuron's resting membrane potential (Control, Mean \pm SD mV, -68.29 ± 5.03 , $n = 24$; Tinnitus, -63.86 ± 6.2 , $n = 14$; $t(36) = 2.4$, $p = 0.021$, t -test) and E. Tinnitus-related decrease in VIP neuron's injected rheobase current (Control, Mean \pm SD pA, 28.33 ± 21.4 , $n = 24$; Tinnitus, 16.92 ± 7.5 , $n = 13$; $p = 0.007$, Mann-Whitney test) recorded from A1 VIP+ neurons in control and tinnitus rats. F. Exemplar traces showing the VIP neurons action potential discharges following injection of twice amplitude rheobase current (2 x RC). G. Plot of number of Action potentials (APs) generated against the rat's normalized tinnitus score (z-score). Action potentials evoked by injecting twice the rheobase current into VIP neurons from control and tinnitus rats (Control, Mean \pm SD APs/2xRC, 0.259 ± 0.05 , $n = 22$; Tinnitus, 0.479 ± 0.15 , $n = 16$; $r^2 = 0.61$, $p = 0.033$). * $p < 0.05$. See methods for z-score normalization.

Table 1:

Animals used in the study

Animals	Wild-type			ChAT-Cre			VIP x tdTomato		
	Control	ET	ENT	Control	ET	ENT	Control	ET	ENT
ABR threshold shift at 16 kHz (Mean dB \pm SD)	3.34 \pm 9.29	18.33 \pm 11.25	17.5 \pm 4.62	5.75 \pm 9.39	11.4 \pm 13.53	13.33 \pm 13.53	2.0 \pm 4.42	22.5 \pm 7.5	13.33 \pm 11.24
Electrophysiological studies (Rats/Neurons)	16/62	19/77	2/12	3/10	5/14	6/25	7/28	6/22	0
Anatomical studies	7	5	2	0	0	0	3	0	3
Total animals used	23	24	4	3	5	6	10	6	3

Author Manuscript

Author Manuscript

Author Manuscript

Author Manuscript

Table 2:

Tinnitus-related changes in cell density across the layers of A1.

Cell Type	L2/3		L4		L5		L6	
	Control	Tinnitus	Control	Tinnitus	Control	Tinnitus	Control	Tinnitus
VGLUT1 (cells/mm ²) ± SD	1267.49 ± 284.37	1320.78 ± 200.45	1142.74 ± 207.09	1180.18 ± 122.60	781.46 ± 268.4	378.82 ± 154.7	953.54 ± 497.64	1060.34 ± 179.34
VGAT (cells/mm ²) ± SD	262.10 ± 79.2	263.14 ± 69.77	380.35 ± 68.22	289.74 ± 65.81	257.27 ± 75.06	256.04 ± 43.98	197.50 ± 49.8	164.15 ± 32.57
PV (cells/mm ²) ± SD	113.68 ± 43.98	116.72 ± 32.10	253.08 ± 89.42	174.59 ± 25.42*	108.26 ± 16.36	126.69 ± 27.35	61.13 ± 24.37	42.58 ± 4.18
VIP (cells/mm ²) ± SD	65.32 ± 17.65	67.52 ± 19.26	30.04 ± 14.69	28.8 ± 18.38	16.87 ± 6.03	15.03 ± 12.44	11.07 ± 5.17	7.29 ± 4.93
SOM (cells/mm ²) ± SD	29.15 ± 10.7	38.68 ± 13.18	80.16 ± 36.56	79.35 ± 20.0	102.22 ± 43.10	86.97 ± 40.28	49.33 ± 16.21	59.04 ± 31.98

* $p < 0.05$, Two-way ANOVA with Bonferroni *post-hoc* correction.